Cofacial Assembly of Partially Oxidized Metallomacrocycles as an Approach to Controlling Lattice Architecture in Low-Dimensional Molecular Solids. Chemical, Structural, Oxidation State, Transport, Magnetic, and Optical Properties of Halogen-Doped [M(phthalocyaninato)O]$_n$ Macromolecules, Where M = Si, Ge, and Sn

Bruce N. Diel,[1a] Tamotsu Inabe,[1a] Joseph W. Lyding,[1b] Karl F. Schoch, Jr.,[1a] Carl R. Kannewurf,*[1b] and Tobin J. Marks*[1a]

Contribution from the Department of Chemistry, the Department of Electrical Engineering and Computer Science, and the Materials Research Center, Northwestern University, Evanston, Illinois 60201. *Received June 7, 1982*

Abstract: This contribution reports an integrated chemical and physicochemical study of the effects of halogen (I_2, Br_2) doping on the cofacially joined metallomacrocyclic polymers [M(Pc)O]$_n$. Resonance Raman and transmission infrared spectroscopy indicates the formation of $([M(Pc)O]^{y/3+}(^1/_3I_3^-)_y)_n$, M = Si, Ge, and $([Si(Pc)O]^{y/3+}(^1/_3Br_3^-)_y)_n$ materials for $y \leq 1.1$. In contrast, for M = Sn, evidence is presented for the destruction of the tin-oxygen bonds upon doping. For M = Si and Ge, the transmission infrared spectra also reveal the progressive growth of electronic absorption with incremental doping; the effect is somewhat stronger for Si than for Ge. Transmission optical spectra of these materials reveal the formation of phthalocyanine π radical cation species and chains of I_3^- counterions. EPR spectra are also in accord with the ligand-centered π radical character of the halogen oxidation. Studies of the doping process (M = Si, Ge) by X-ray diffractometry indicate that it is inhomogeneous and that a single, limiting phase of stoichiometry $y \approx 1.1$ is produced upon halogenation. Structural characterization of the $([Si(Pc)O]I_{1.12})_n$, $([Ge(Pc)O]I_{1.12})_n$, and $([Si(Pc)O]Br_{1.12})_n$ phases by computer analysis of the diffraction data (supported by judiciously selected model compounds) indicates architectural motifs that are essentially isomorphous with Ni(Pc)I, i.e., stacks of staggered M(Pc) units and parallel chains of I_3^- counterions. The data can be indexed in space group $P4/mcc$, $Z = 2$, with $a = 13.936$ (6) Å, $c = 6.488$ (3) Å, phthalocyanine staggering angle = 39.5° (Ni); $a = 13.97$ (5) Å, $c = 6.60$ (4) Å, staggering angle = 39 (3)° (M = Si); $a = 13.96$ (5) Å, $c = 6.96$ (4) Å, staggering angle = 40 (4)° (M = Ge). Evidence is presented that the I_3^- (or Br_3^-) counterions are disordered along c. Variable-temperature static magnetic susceptibility studies of the $([M(Pc)O]I_y)_n$ polymers reveal a small, sample-dependent Curie component and a Pauli-like, weakly temperature-dependent contribution. The magnitude of the latter is linearly proportional to y and can be associated with the fully doped, $y \approx 1.1$ phase. The magnitude of the Pauli-like component increases with increasing interplanar ring-ring spacing (Ni → Si → Ge) while bandwidths ($4t$) calculated on the basis of a simple tight-binding model decrease. High-resolution ^{13}C NMR spectra (^1H decoupled with cross-polarization and magic angle spinning) reveal a downfield shift of $[Si(Pc)O]_n$ carbon resonances upon doping. Optical reflectivity studies of the M = Si and Ge materials reveal the development of a plasma-like edge in the infrared upon incremental doping with iodine (the effect is stronger for Si than for Ge). Comparison of the data for Ni(Pc)I, $([Si(Pc)O]I_{1.12})_n$, and $([Ge(Pc)O]I_{1.12})_n$ reveals the progressive shift of the edge to lower energy with increasing interplanar spacing (Ni → Si → Ge). This trend is paralleled by plasma frequencies (ω_p) derived from a Drude analysis and tight-binding bandwidths calculated therefrom. Four-probe electrical conductivity measurements for polycrystalline samples of the Si and Ge polymers reveal a sharp increase in conductivity upon incremental iodine doping. The functional form of the σ vs. y plot can be fit to a simple percolation model, in accord with the inhomogeneous character of the doping. For the fully doped materials, the compaction conductivity inversely correlates with the ring-ring interplanar spacings, viz., $\sigma_{Ni} > \sigma_{Si} > \sigma_{Ge}$. The temperature dependence of the conductivity data (4.2-300 K) indicates a region of falling $d\sigma/dT$ for M = Ni and Si, suggesting "metal-like" charge transport in the stacking direction near room temperature (already established for M = Ni), while the M = Ge material does not exhibit such behavior. The conclusion for $([Si(Pc)O]I_{1.12})_n$ is supported by voltage-shorted compaction measurements. The temperature dependence of the M = Ni, Si and Ge powder conductivity data can best be fit to a transport model involving fluctuation-induced carrier tunneling through parabolic potential barriers that separate the high conductivity regions.

In the preceding contribution[2] we discussed the chemical, spectroscopic, and structural properties of the cofacially joined group 4A phthalocyaninato macromolecules [M(Pc)O]$_n$, where M = Si, Ge, Sn. Arrayed in a rigorously enforced stacking pattern and at variable, controlled distances are molecular donor subunits which, in ideal cases (e.g., Ni(Pc) doped with iodine[3]), have been shown to be precursors for highly conductive "molecular metals".[4] Such assemblies[5] offer an intriguing opportunity to probe in the presence of a fixed acceptor species, the response of an array of relatively constant, well-characterized donor subunits to certain deliberate modifications in stacking architecture and stacking

(1) (a) Department of Chemistry. (b) Department of Electrical Engineering and Computer Science.

(2) Dirk, C. W.; Inabe, T.; Schoch, K. F., Jr.; Marks, T. J. *J. Am. Chem. Soc.* **1983**, *105* (preceding paper in this issue).

(3) (a) Schramm, C. S.; Scaringe, R. P.; Stojakovic, D. R.; Hoffman, B. M.; Ibers, J. A.; Marks, T. J. *J. Am. Chem. Soc.* **1980**, *102*, 6702-6713. (b) Marks, T. J.; Kalina, D. W. In "Extended Linear Chain Compounds"; Miller, J. S., Ed.; Plenum Press: New York, 1982; Vol. 1 pp 197-331. (c) Stojakovic, D. R. Ph.D. Thesis, Northwestern, University, 1978. (d) Inabe, T.; Lyding, J. W.; Moguel, M. K.; Kannewurf, C. R.; Marks, T. J. *J. Mol. Cryst. Liq. Cryst.*, in press.

(4) (a) Miller, J. S., Ed. "Extended Linear Chain Compounds"; Plenum Press: New York, 1982; Vol. 1,2. (b) Alcăcer, L., Ed. "The Physics and Chemistry of Low-Dimensional Solids"; D. Reidel: Dordrecht, 1980. (c) Devreese, J. T.; Evrard, V. E.; Van Doren, V. E., Eds. "Highly Conducting One-Dimensional Solids"; Plenum Press: New York, 1979. (d) Hatfield, W. E., Ed. "Molecular Metals"; Plenum Press: New York, 1979. (e) Torrance, J. B. *Acc. Chem. Res.* **1979**, *12*, 79-86. (f) Miller, J. S.; Epstein, A. J., *Ann. N.Y. Acad. Sci.* **1978**, *313*. (g) Keller, H. J., Ed. "Chemistry and Physics of One-Dimensional Metals"; Plenum Press: New York, 1977.

(5) (a) For results on isoelectronic group 3A [M(Pc)F]$_n$ materials, see: Nohr, R. S.; Kuznesof, P. M.; Wynne, K. J.; Kenney, M. E.; Siebenman, P. G. *J. Am. Chem. Soc.* **1981**, *103*, 4371-4377. (b) For results on similar [M(Pc)L]$_n$ materials where L is a bridging organic ligand and M is a transition metal, see: Schneider, O.; Hanack, M. *Angew. Chem., Int. Ed. Engl.* **1982**, *21*, 79 and references therein.

0002-7863/83/1505-1551$01.50/0

Table I. Elemental Analytical Data for $([M(Pc)O]I_y)_n$ and $([M(Pc)O]Br_y)_n$ Materials

	calcd				found			
y	C	H	N	X	C	H	N	X
				$([Si(Pc)O]I_y)_n$				
0.12	67.21	2.82	19.59	2.66	66.17	2.80	19.32	2.60
0.23				4.94				4.94
0.31				6.53				6.53
0.71				13.89				13.89
1.12				20.33				20.33
1.15	54.71	2.30	15.95	20.77	54.50	2.30	15.95	20.77
				$([Si(Pc)O]Br_y)_n$				
0.90	61.15	2.57	17.83	11.44	60.61	2.87	17.74	10.34
1.82				20.75				20.75
				$([Ge(Pc)O]I_y)_n$				
0.14	62.10	2.60	18.10	2.87	62.23	2.66	18.06	2.96
0.31				6.08				6.08
0.56				10.53				10.53
1.07	52.70	2.21	15.36	17.58	52.01	2.17	15.13	17.57
1.12				19.20				19.20
				$([Sn(Pc)O]I_y)_n$				
0.14	57.80	2.43	16.85	2.67	55.48	2.38	15.80	2.72
0.32				5.84				5.84
0.60				10.49				10.49
1.11				17.86				17.86
1.76	44.15	1.85	12.87	25.65	41.26	1.91	11.74	25.63

restoring forces. Furthermore, it will be seen that such metallomacrocyclic materials allow certain lines of experimentation heretofore impossible with existing classes of electrically conductive polymers.[6] In the present article we focus in depth on the chemical, structural, oxidation state, charge transport, magnetic, and optical response of the $[M(Pc)O]_n$ metallomacrocyclic array to doping by halogen (principally iodine) oxidants.

Experimental Section

General synthetic manipulations and solvent purifications were as described in the accompanying article.[2] The $[M(Pc)O]_n$ materials were prepared as described in ref 2. The $[Si(Pc)O]_n$ samples included specimens polymerized at 440 °C (10^{-3} torr) for both 1 and 12 h, the $[Ge(Pc)O]_n$ samples, specimens polymerized at 440 °C (10^{-3} torr) for 10 and 48 h. Ni(Pc)I was prepared as described elsewhere.[3] Iodine was triply sublimed.

Synthesis of $([M(Pc)O]I_y)_n$ and $([M(Pc)O]Br_y)_n$ Materials. Halogen-doped polymers were prepared by finely powdering the $[M(Pc)O]_n$ precursors in a mortar and pestle and then stirring for 48 h with a solution of the appropriate halogen in dry, deoxygenated benzene. At low doping levels, the supernatant soon became colorless. The black product was isolated by centrifugation, washed with several portions of benzene, and dried for 1 h under high vacuum (10^{-3} torr). For incremental doping investigations, a portion of isolated, doped material was reserved for analysis and physical measurements, while the remainder was reacted with additional halogen. It was also found that doping could be achieved with I_2 vapor in a sealed container at 80–100 °C or, in the case of $[Si(Pc)O]_n$, by dissolving the polymer in concentrated H_2SO_4 and filtering the solution through a glass frit into an aqueous I_2/I^- solution. For a given dopant level, the conductivity was not significantly affected by the doping methodology, although the solution method provided the best control over the amount of halogen incorporated. Analytical data for $([M(Pc)O]I_y)_n$ and $([M(Pc)O]Br_y)_n$ materials prepared are summarized in Table I. Neither $Si(Pc)Cl_2$ nor $Si(Pc)(OH)_2$ absorbed detectable quantities of I_2 under standard doping conditions.

Raman Spectroscopy. Raman spectra of the halogen-doped polymers were recorded with Ar^+ excitation (5145 Å), using a Spex 1401 monochromator and photon counting detection. Calibration was with the laser exciting line or plasma emissions. The samples were studied as powders in 5-mm Pyrex tubes spinning at 1200 rpm with a 180° backscattering geometry. There was no evidence of decomposition after multiple scans on individual samples.

Transmission Infrared Spectroscopy. Transmission infrared spectra of halogen-doped polymers were recorded on Nujol mulls between KBr plates with Perkin-Elmer Model 283 or 599-B spectrometers and were calibrated with polystyrene film. Multiple scans were performed to check for possible decomposition.

Transmission Optical Spectroscopy. Transmission optical spectra were recorded on Nujol mulls between quartz plates with a Perkin-Elmer Model 330 spectrophotometer and associated data system. Several scans were routinely made to verify that no decomposition was occurring.

Reflectance Spectroscopy. The reflectance spectra of $[M(Pc)O]_n$ and $([M(Pc)O]I_y)_n$ materials in the frequency range 100–4000 cm^{-1} were recorded with a Perkin-Elmer Model 180 infrared spectrophotometer. The instrument was operated in the double-beam mode and adjusted to yield a resolution of approximately 1.0 cm^{-1} at 4000 cm^{-1}. A mercury source and pyroelectric detector were used in the frequency range 100–525 cm^{-1}, while in the range 300–4000 cm^{-1} a globar source and thermopile were employed. Calibration of this instrument was accomplished by means of a front surface gold mirror. For measurements above 4000 cm^{-1} a Zeiss MM-12 monochromator was used in conjunction with a PbS detector for frequencies less than 16 000 cm^{-1} and a photomultiplier detector in the frequency range 16 000–50 000 cm^{-1}. For frequencies less than 30 000 cm^{-1} a tungsten source was used, while a deuterium source was used at higher frequencies. Slit widths were adjusted such that the resolution at all frequencies was better than 1%, and calibration of this instrument was accomplished by use of a front surface aluminum mirror. Continuity between the two instruments was obtained by overlapping mirror calibrations from 3600 to 4400 cm^{-1}. All measurements were made at room temperature with unpolarized radiation and at near-normal incidence for both instruments.

The samples, which were prepared as described for the electrical transport measurements, were pressed (with polished dies) polycrystalline pellets in the shape of flat disks, 13 mm in diameter with thicknesses of 0.75–1.0 mm. In all arrangements, the area of the incident light beam was much less than the area of the sample; the reflective quality of the front surface showed no appreciable variation across the surface area. Data analysis employed the computer program described previously.[7a]

Charge-Transport Measurements. Direct current electrical conductivity measurements were obtained for pressed pellet powder compactions of the undoped and doped polymers over the range $4.2 \leq T \leq 320$ K. A computer controlled system was employed to provide automated temperature control, data acquisition, and programmed as well as operator real-time decision-making capabilities.[7b] This system utilizes a dipstick providing electrical and thermal connections into which individual sample holders are interchangeably connected. The number of electrical con-

(6) (a) Wynne, K. J.; Street, G. B. *Ind. Eng. Chem. Prod. Res. Dev.* **1982**, *21*, 23–28. (b) Baughman, R. H.; Brēdas, J. L.; Chance, R. R.; Elsenbaumer, R. L.; Shacklette, L. W. *Chem. Rev.* **1982**, *82*, 209–222. (c) Wegner, G. *Angew. Chem., Int. Ed. Engl.* **1981**, *20*, 361–381. (d) Duke, C. B.; Gibson, H. W. In "Kirk-Othmer Encyclopedia of Chemical Technology", 3rd ed.; Wiley: New York, 1982; Vol. 18, 755–793. (e) Seymour, R. B., Ed. "Conductive Polymers", *Polym. Sci. Technol.* **1981**, *16*.

(7) (a) Ratajack, M. T.; Kishio, K.; Brittain, J. O.; Kannewurf, C. R. *Phys. Rev. B: Condens. Matter* **1980**, *B21*, 2144–2149. (b) Lyding, J. W.; Kannewurf, C. R., submitted for publication. (c) Seeger, K. "Semiconductor Physics"; Springer-Verlag: New York, 1973; pp 482–488. (d) Smits, F. M. *Bell Syst. Tech. J.* **1958**, 711–718.

nections allows for up to eight samples to be placed on a single sample holder in either a conductivity (four-probe)[7c,d] or Hall effect (five-probe) arrangement and thus to be measured in a single experimental run. For this study, a sample holder was designed to accommodate the particular specimen geometry (1 × 1 × 5 mm pellets or 13 × 2 mm disks) and to facilitate making ohmic contacts. The material to be measured was ground in a mortar and pestle and then transferred to the pellet die and pressed under 8–10 tons of pressure in a ring press. Sample pellets were mounted on a glass coverslip which was affixed to a copper heat sink by vacuum grease. Electrical connections were accomplished with 5-mil tungsten wires spring-loaded across the pellet surface and further joined with conductive gold paste or Aquadag. Contact separations were measured with a calibrated binocular microscope. Routinely, three to four specimens were processed for a given sample stoichiometry. The agreement between measured conductivity values was typically within ±2% of the mean. After the pellets were mounted, the sample holder was hermetically sealed to prevent dopant loss resulting from the high vacuum environment of the dipstick.

Before initiating a variable-temperature measurement sequence, samples were screened at room temperature for ohmic behavior, low contact resistance, and any time-dependent behavior. For liquid nitrogen runs, the temperature sequencing was programmed to cycle from room temperature to 80 K (typically in 2 K steps) and then return to above room temperature (320 K). For liquid helium runs, samples were precooled to 4.2 K and then brought up to 100 K in intervals ranging from 0.2 to 2 K. Stable temperature control (±0.01 K) was established at each set point before data acquisition was initiated. Typically, three to four separate variable-temperature runs were carried out for each specimen to check for reproducibility and reversibility. At a given temperature, reproducibility was within 5%.

The system incorporates sample selection and choice of two distinct configurations of source and measurement electronics into the experimental software operating system to provide truly automated DC measurements. The configuration used for sample resistances in the range $0 \leq R \leq 10^5\ \Omega$ consists of a Keithley 225 current source and a Keithley 174 autoranging DVM. The corresponding instruments for high resistance measurements ($10^5 < R \leq 10^{12}\ \Omega$) are a Kethley 640 vibrating capacitor electrometer (current measurement) and a Keithley 604 differential electrometer used in conjunction with another Keithley 225 current source.

The sample resistance in the charge transport analysis system is determined from the usual procedure of averaging the results obtained for voltages recorded before and after reversing the current direction through the sample. In addition, individual current and voltage values are comprised of a sequence of samples the number of which is dependent upon the signal level involved. Also, this measurement sequence is initiated only after the monotonic time constant voltage drift associated with high resistance measurements has subsided. A time limit corresponding to $10^{12}\ \Omega$ is incorporated to prevent any undue delay from a defective sample (e.g., electrode open circuit). During the course of the experiment, all of the raw data (raw data being the mean and standard deviation of a sampled sequence) are stored on disk along with the calculated sample resistivity. These data are used in conjunction with the reproducibility of results between separate experiments as criteria for judgment of the quality of the results obtained.

ESR Spectroscopy. Electron spin resonance experiments were carried out on a highly modified Varian E-4 X-band ESR spectrometer with 100-kHz field modulation. The field was calibrated with 2,2-phenyl-1-picrylhydrazyl (DPPH, $g = 2.0036$). The cavity resonance frequency was measured to an accuracy of 5 ppm by a transfer oscillator technique.

Magnetic Susceptibility Measurements. Static magnetic susceptibilities were measured from 6 to 340 K with a S.H.E. VTS-10 SQUID susceptometer. Samples were contained in a closed Si–Al alloy "bucket"; experiments with and without the bucket cap and using varying pump-down procedures indicated that the effects of adsorbed oxygen were negligible. The instrument calibration was checked with $HgCo(SCN)_4$. Measurements were routinely performed at 5 kG; experiments as a function of field indicated that the effects of ferromagnetic impurities in the $([M(Pc)O]I_y)_n$ materials were not significant. Ample time was allowed for sample equilibration at each new temperature. For polymer ($[M(Pc)O]_n$) diamagnetic corrections, twice the tabulated[8a,b] Pascal constant for chlorine (-40.2×10^{-6} emu mol^{-1}) was subtracted from and the tabulated[8a,b] Pascal constant for oxygen (-4.6×10^{-6} emu mol^{-1}) added to the measured susceptibilities of freshly sublimed $Si(Pc)Cl_2$ (-4.908×10^{-4} emu mol^{-1}), $Ge(Pc)Cl_2$ (-4.480×10^{-4} emu mol^{-1}), and $Sn(Pc)Cl_2$ (-4.516×10^{-4} emu mol^{-1}) samples.[9] These parameters were used in preference to the experimental susceptibilities of the $[M(Pc)O]_n$ compounds since it was not possible to ensure that these latter materials were not already partially oxidized as a result of the synthetic procedure, and it was not possible to purify them to the same extent as for the corresponding dichlorides. There was good agreement between the calculated and observed susceptibilities of the dichlorides.[9b]

The diamagnetic correction for I_3^- was approximated from the sum of twice that for $I(-44.6 \times 10^{-6}$ emu mol$^{-1})$ and that for I^- (-50.6×10^{-6} emu mol^{-1}).[8c] The Curie components of all variable-temperature data sets were analyzed in a χ vs. $1/T$ format, using linear regression techniques.

High-Resolution Solid-State ^{13}C NMR Spectroscopy. ^{13}C NMR spectra of $[M(Pc)O]_n$ and $([Si(Pc)O]I_y)_n$ materials were obtained on a JEOL FX60-QS spectrometer operating at 15.1 MHz, employing ^1H decoupling with cross-polarization and magic angle spinning techniques. Care was taken to achieve optimum pulse width, pulse delay, Harmann–Hahn contact time, and magic angle setting. Typical parameters were ^1H pulse width = 5.5 μs (90°), contact time = 3.0 ms, and pulse delay = 5.0 s. Typical spectra required 1000–8000 acquisitions. Several spectra were also obtained with a Bruker CXP-200 spectrometer and were qualitatively similar. We thank Dr. D. R. Müller (Bruker Analytische Masstechnik, GMBH) for these spectra.

X-ray Diffraction. X-ray powder diffractometry was carried out with a Rigaku Geigerflex instrument, using Ni-filtered Cu Kα radiation and the sampling techniques described previously.[2] Local versions of the programs INDX, POLSQ, and LAZY PULVERIX[2] were employed for data analysis. Preferred crystallite orientation was also examined by diffractometric techniques. Since the high linear absorption coefficients and fragility of very thin pellets adversely affected the accuracy of transmission measurements,[10a] analysis was carried out from reflection data obtained parallel to and perpendicular to the pellet compression direction.[2] By comparing the relative intensities of the 002 reflections and considering possible orientation spheres,[10b] it was possible to obtain orientation information expressed as the mean-square cosine of the angle (α) between the crystallographic c axis and the pellet compression direction (z). These are $\langle\cos^2 \alpha_{c,z}\rangle = 0.25$ (3) for Ni(Pc)I, 0.27 (2) for $([Si(Pc)O]I_{1.12})_n$, and 0.33 (1) (random orientation) for $([Ge(Pc)O]I_{1.12})_n$. Densities were measured by the previously discussed aqueous $ZnCl_2$ flotation procedures.[2]

Results

There are several issues of central importance in understanding how the different $[M(Pc)O]_n$ polymers interact with halogens and how this chemistry impacts upon collective properties. First, whether or not macrocycle oxidation is occurring and the electronic/molecular structures of the halogenation products are crucial data. Second, and a topic of considerable current controversy in most conductive polymer systems,[6,8c,11] is the question of whether the doping is homogeneous, i.e., whether the dopant species distribute themselves uniformly throughout the solid as doping progresses or whether discrete phases of definite stoichiometry coexist. We begin with a discussion of the chemistry and structural changes accompanying the introduction of halogen. We then discuss the magnetic, optical, and transport properties as a function of M and dopant level. Finally, we interpret these observations and trends in light of what is presently known about both stacked molecular systems and other electrically conductive, doped polymers. In this study, materials with relatively high degrees of polymerization (average $n > 50$) were employed. In this range, polymer physical properties appear not to be highly sensitive to chain length. This is not true for lower molecular weights, and this fascinating question will be taken up in a subsequent contribution.[12a]

(8) (a) Earnshaw, A. "Introduction to Magnetochemistry"; Academic Press: London, 1968; pp 4–8. (b) Mulay, L. N. In "Theory and Applications of Molecular Diamagnetism"; Mulay, L. N., Boudreaux, E. A., Eds.; Wiley-Interscience: New York, 1976; Chapter 5.3. (c) From CsI_3, the correction for I_3^- is determined to be -43.6×10^{-6} emu mol^{-1} I: Epstein, A. J.; Rommelmann, H.; Druy, M. A.; Heeger, A. J.; MacDiarmid, A. G. *Solid State Commun.* **1981**, *38*, 683–687.

(9) (a) Small Curie tails (~0.1% paramagnetic, $S = {}^1/_2$ impurities) were detected and subtracted out by linear regression techniques. (b) For example, the calculated susceptibility of $Si(Pc)Cl_2$ is -4.63×10^{-3} emu mol^{-1}.

(10) (a) Alexander, L. E. "X-ray Diffraction Methods in Polymer Science"; Wiley: New York, 1969; pp 209–240. (b) *Ibid.*; pp 241–252.

(11) (a) Tomkiewicz, Y.; Schultz, T. D.; Broom, H. B.; Clark, T. C.; Street, G. B. *Phys. Rev. Lett.* **1979**, *43*, 1532–1536. (b) Mortensen, K.; Thewalt, M. L. W.; Tomkiewicz, Y.; Clarke, T. C.; Street, G. B. *Ibid.* **1980**, *45*, 490–495.

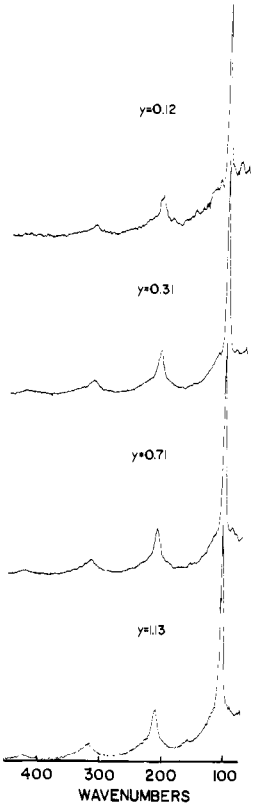

Figure 1. Resonance Raman spectra (ν_0 = 5145 Å) of $([Si(Pc)O]I_y)_n$ doped with varying amounts of iodine.

$[M(Pc)O]_n$ Doping Chemistry. The $[M(Pc)O]_n$ materials can be doped with dissolved or gaseous halogen (most experiments were conducted with I_2) as shown in eq 1. In the case of [Si-

$$[M(Pc)O]_n + ny/2X_2 \rightarrow ([M(Pc)O]X_y)_n \quad (1)$$

$$M = Si, Ge, Sn; X = Br, I$$

$(Pc)O]_n$, doping could also be achieved by dissolving the polymer in concentrated sulfuric acid and precipitating it with aqueous I^-/I_2. Materials which were prepared are given in Table I. Although stoichiometries with y as high as 2–3 could be achieved, when the workup procedure involved vacuum drying for 1 h, the isolated stoichiometries never exceeded $y \approx 1.1$ for M = Si and Ge. Several lines of evidence indicate that the doping process is somewhat more complicated for $[Sn(Pc)O]_n$ (vide infra). As monitored by Raman spectroscopy and elemental composition, attempts to dope $Si(Pc)Cl_2$ and $Si(Pc)(OH)_2$ by the usual procedure did not result in iodine uptake.

$([M(Pc)O]I_y)_n$ and $([M(Pc)O]Br_y)_n$ Resonance Raman Spectroscopy. Resonance Raman spectroscopy was employed to monitor, via established structure–spectra criteria,[3b,12b,c] the form(s) of iodine present as the $[M(Pc)O]_n$ macromolecules were progressively doped. As exemplified by M = Si (Figure 1), the characteristic, totally symmetric (ν = 108 cm^{-1}) scattering pattern (and accompanying overtone progression) of I_3^- is observed at even the lowest doping levels. Clearly, oxidation of the phthalocyanine array is occurring. Incremental addition of iodine results only in more intense I_3^- scattering up to $y \approx 1.1$. Beyond this point, a transition at 165 cm^{-1}, attributable to I_5^-[12,13] is also evident for the Si and Ge polymers. Figure 2 compares typical $([Si(Pc)O]I_y)_n$ resonance Raman data, $y \approx 1.1$, to those for the corresponding

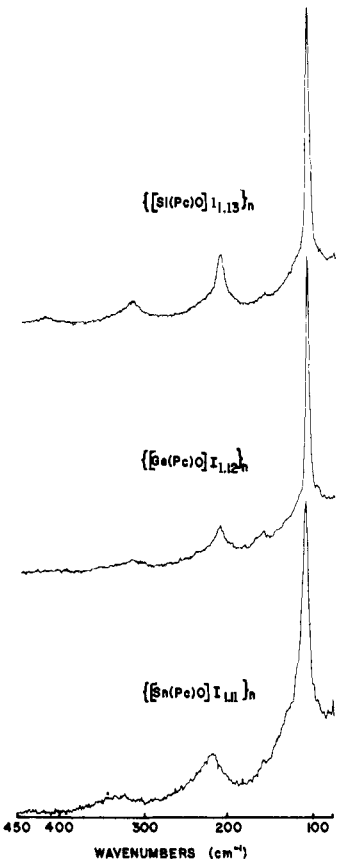

Figure 2. Resonance Raman spectra of several $([M(Pc)O]I_y)_n$ materials (ν_0 = 5145 Å).

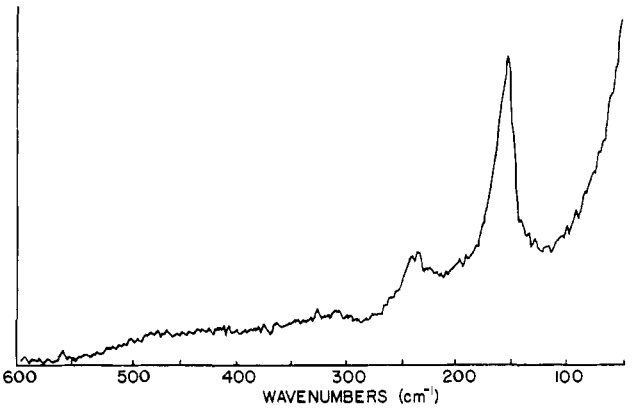

Figure 3. Resonance Raman spectrum of $([Si(Pc)O]Br_{1.8})_n$ (ν_0 = 5145 Å).

Ge and Sn polymers. In the case of the $([Sn(Pc)O]I_y)_n$ materials, levels of I_2 up to $y \approx 2$ are required before I_5^- is evident in the Raman spectra. Scattering from free I_2 ($\nu_{I-I} \approx 205$ cm^{-1}) is never observed in $([M(Pc)O]I_y)_n$ samples.

Bromine doping was only investigated to a limited extent (Table I). Resonance Raman spectra indicate that oxidation of the metallomacrocyclic stack is again occurring. For $([Si(Pc)O]-Br_{1.8})_n$, both Br_3^- (ν_{symm} = 164 cm^{-1} along with overtones) and Br_5^- (ν = 241 cm^{-1})[14] are evident (Figure 3), and at stoichiometries where $y < 1.1$, only Br_3^- is detected. Free Br_2 (ν = 306 cm^{-1})[14] is not detected in any brominated samples.

$([M(Pc)O]I_y)_n$ Transmission Infrared Spectroscopy. Solid-state infrared spectra of the siloxane, germyloxane, and stannyloxane compounds were studied as a function of iodine dopant level

(12) (a) Inabe, T.; Lyding, J. W.; Kannewurf, C. R.; Marks, T. J., manuscript in preparation. (b) Teitelbaum, R. C.; Ruby, S. L.; Marks, T. J. *J. Am. Chem. Soc.* **1980**, *102*, 3322–3328. (c) Teitelbaum, R. C.; Ruby, S. L.; Marks, T. J. *Ibid.* **1979**, *101*, 7568–7573.

(13) Cowie, M. A.; Gleizes, A.; Grynkewich, G. W.; Kalina, D. W.; McClure, M. S.; Scaringe, R. P.; Teitelbaum, R. C.; Ruby, S. L.; Ibers, J. A.; Kannewurf, C. R.; Marks, T. J. *J. Am. Chem. Soc.* **1979**, *101*, 2921–2936.

(14) Kalina, D. W.; Lyding, J. W.; Ratajack, M. T.; Kannewurf, C. R.; Marks, T. J. *J. Am. Chem. Soc.* **1980**, *102*, 7854–7862.

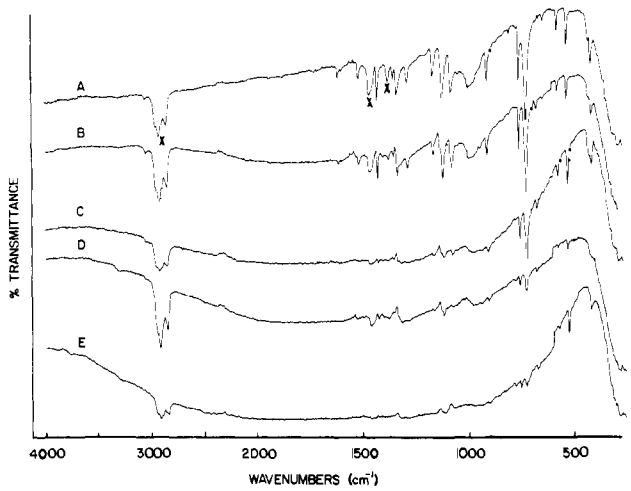

Figure 4. Transmission infrared spectra of $([Si(Pc)O]I_y)_n$: (A) $y = 0.00$; (B) $y = 0.12$; (C) $y = 0.36$; (D) $y = 0.71$; (E) $y = 1.13$. Transitions denoted with an x are due to Nujol.

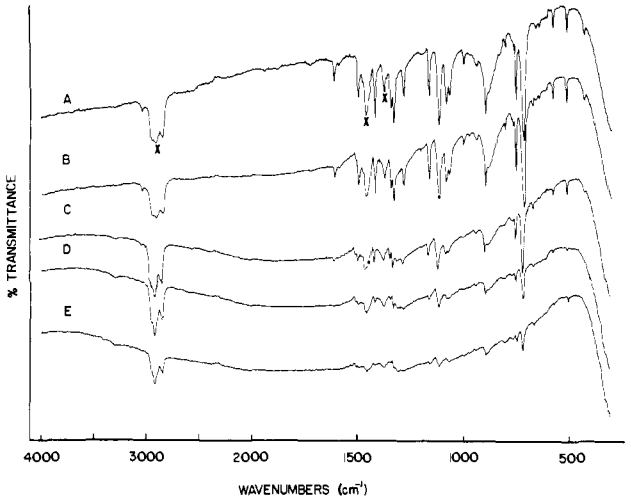

Figure 5. Transmission infrared spectra of $([Ge(Pc)O]I_y)_n$: (A) $y = 0.00$; (B) $y = 0.14$; (C) $y = 0.3$; (D) $y = 0.56$; (E) $y = 1.12$. Transitions denoted with an x are due to Nujol.

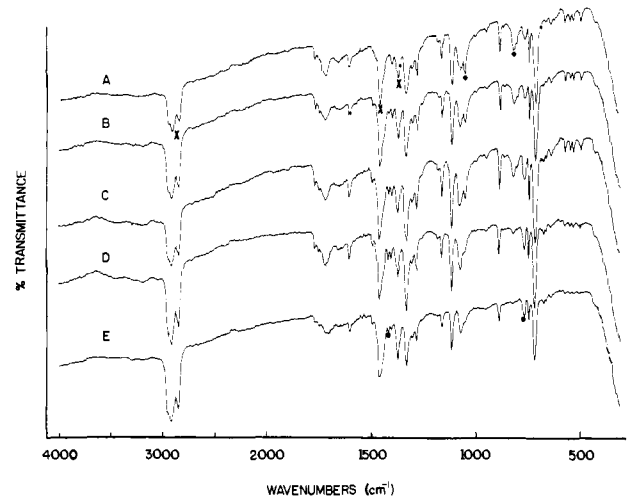

Figure 6. Transmission infrared spectra of $([Sn(Pc)O]I_y)_n$: (A) $y = 0.00$, (B) $y = 0.32$; (C) $y = 0.60$; (D) $y = 1.11$; (E) $y = 1.76$. Transmission denoted with an x are due to Nujol. Absorbances marked (●) in A disappear on doping and those marked (●) in E grow in on doping.

(Figures 4–6). In the case of M = Si, a broad, intense absorption centered at ca. 1800 cm^{-1} is observed to grow in as the iodine level increases. Such features are typical of highly conductive molecular

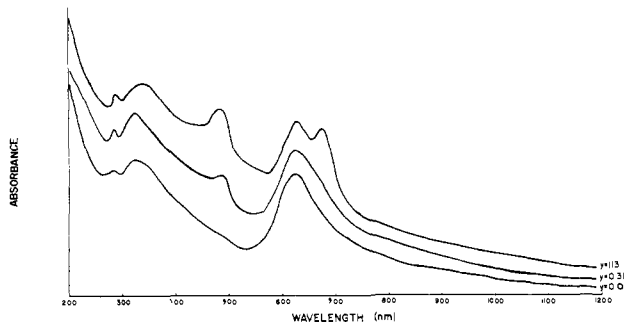

Figure 7. Transmission optical spectra of $([Si(Pc)O]I_y)_n$ compounds as Nujol mulls.

Table II. Solid-State Electronic Absorption Data for $([M(Pc)O]I_y)_n$ Compounds[a]

y	absorption maxima, nm
	$([Si(Pc)O]I_y)_n$
0.00	203, 285, 335, 625
1.13	203, 285, 335, 490, 630, 680
	$([Ge(Pc)O]I_y)_n$
0.00	285, 350, 645
1.12	210, 290, 340, 490, 650, 680
	$([Sn(Pc)O]I_y)_n$
0.00	205, 290, 365, 655, 695
1.76	295, 370, 500 sh, 660 sh, 690

[a] As Nujol mulls.

and macromolecular materials and arise from conduction electron excitation.[5a,6,15] They are not observed in simple organic polyiodides.[3b] Other than diminution of intensity, there are no detectable displacements in the phthalocyanine skeletal or Si–O chain modes[16] greater than ±7 cm^{-1} and no unambiguous evidence for the appearance of new, infrared-active, vibrational modes. There are no features that would indicate disruption of the cofacially joined metallomacrocyclic architecture. It will be seen on the basis of other physicochemical data (vide infra) that the undoped $[Si(Pc)O]_n$ and $[Ge(Pc)O]_n$ phases are consumed by $y \approx 1.1$. In the case of $[Ge(Pc)O]_n$, a very broad electronic absorption is also apparent upon doping (Figure 5); however, for the same iodine stoichiometry, the effect is somewhat weaker than for $([Si(Pc)O]I_y)_n$. Thus, relative to the ring mode at 750 cm^{-1}, the electronic absorption in the infrared is ca. 3 times more intense for $([Si(Pc)O]I_{1.13})_n$ than for $([Ge(Pc)O]I_{1.12})_n$. As in the silicon system, any shifts of the M(Pc) or M–O vibrational modes upon doping are less than ±7 cm^{-1} and there is no clear indication of new modes or that the basic polymer structure has been altered. Further comparisons will be drawn in the discussion of the optical reflectance data (vide infra).

In the case of $[Sn(Pc)O]_n$ doping by iodine, the infrared data (Figure 6) do not reveal the presence of electronic absorption. Furthermore, the molecular modes at 825 and 1058 cm^{-1} disappear while the absorptions at 770 and 1420 cm^{-1} increase in relative intensity. These changes appear not to be characteristic of phthalocyanine radical cation formation,[17] but rather alteration or destruction of the Sn–O bond, since the 825-cm^{-1} transition was assigned[2] to the locally antisymmetric[16] O–Sn–O stretching mode. In view of the high reactivity of Sn–O–Sn functionalities,[18]

(15) (a) Bozio, R.; Pecile, C. in ref 4b; pp 165–186. (b) Fincher, C. R., Jr.; Ozaki, M.; Heeger, A. J.; MacDiarmid, A. G. *Phys. Rev. B: Condens. Matter* **1979**, *B19*, 4140–4148. (c) Wheland, R. C.; Gillson, J. L. *J. Am. Chem. Soc.* **1976**, *98*, 3916–3925. (d) Tanner, D. B.; Jacobsen, C. S.; Garito, A. F.; Heeger, A. J. *Phys. Rev. B: Condens. Matter* **1976**, *B13*, 3381–3404. (e) Perez-Albuerne, E. A.; Johnson, H., Jr.; Trevoy, D. J. *J. Chem. Phys.* **1971**, *55*, 1547–1554.

(16) Formally, these modes should be represented by the optical branch of a dispersion relation rather than local "group vibrations".[2]

(17) Myers, J. F.; Canham, G. W. R.; Lever, A. B. P. *Inorg. Chem.* **1975**, *14*, 461–468.

Table III. Powder EPR Data for Iodinated Phthalocyanine Face-to-Face Polymers

compd	temp, K	g	Γ,[a] G
$([Si(Pc)O]I_{1.13})_n$	298	2.0054[b]	2.9
	77	2.0047[b]	3.1
$([Ge(Pc)O]I_{1.07})_n$	298	2.0074, 2.0059	ca. 3.8, 2.0[c]
	77	2.0078, 2.0058	ca. 5.6, 3.5[c]
$([Sn(Pc)O]I_{1.20})_n$	298	2.002	6.0

[a] Observed line width. [b] Averaged g value; $g_\parallel$ and $g_\perp$ are not resolved. [c] Overlapping signals.

such reactivity is not completely unanticipated.

$([M(Pc)O]I_y)_n$. Transmission Optical Spectroscopy. As noted in ref 2, the optical spectra of the $[M(Pc)O]_n$ polymers are readily understandable in terms of what is known about mononuclear metallophthalocyanine spectra.[19] Significant changes are noted upon incremental iodine doping. As can be seen for M = Si in Figure 7, the major changes are the development of absorption in the α-band region at ca. 680 nm and the appearance of a new band at 490 nm. The changes in the $[Ge(Pc)O]_n$ and $[Sn(Pc)O]_n$ electronic spectra upon iodination are essentially identical (Table II). Upon π radical cation formation, phthalocyanine optical spectra are known to exhibit broadening or splitting in the α-band region, with a red shift on the order of 100–150 nm.[17,20] Thus, the present spectral features can be interpreted in terms of metallomacrocycle oxidation and the formation of a π radical cation electronic structure. This conclusion will be supported by EPR data (vide infra). Similar spectral changes were noted in the iodine doping of Ni(Pc).[3a]

The $([M(Pc)O]I_y)_n$ optical transition at 490 nm can be assigned to an array of I_3^- counterions. In solution or as isolated units in the solid state, I_3^- exhibits transitions (probably $\sigma_g \rightarrow \sigma_u^*$ split by spin–orbit coupling) at higher energy (288 and 352 nm in aqueous solution, ca. 310 and 360 nm in the solid).[3b,21] However, in arrays such as the linear triiodide chains in $(benzamide)_2H^+I_3^-$, the maximum is displaced to ca. 500 nm.[3b,21a] A similar assignment was made for Ni(Pc)I,[3b] which also possesses linear I_3^- chains, in this case extending parallel to the Ni(Pc) stacking direction. Chains of I_5^- result in displacement of the absorption maximum to even longer wavelengths.[3b,13,21a]

$([M(Pc)O]I_y)_n$ Magnetism. Electron Paramagnetic Resonance. The nature of the partially oxidized state was also probed by EPR spectroscopy. Studies of the $([M(Pc)O]I_y)_n$ powders revealed nearly free electron g values and largely isotropic line shapes, consistent with unpaired spin density in molecular orbitals which are predominantly ligand in character.[20] An analogous conclusion was drawn for Ni(Pc)I.[3a] EPR data are set out in Table III.

X-ray Diffraction. The Doping Process and Structural Considerations. As discussed in the accompanying contribution,[2] all structure-sensitive physicochemical data for the $[M(Pc)O]_n$ polymers are in accord with a cofacially arrayed metallomacrocycle polymer architecture and crystal structures composed of parallel arrangements of these rodlike macromolecules. As evidenced by X-ray powder diffractometry, profound structural changes occur upon incremental doping with iodine. Data for $[Si(Pc)O]_n$ and $[Ge(Pc)O]_n$ are illustrated in Figures 8 and 9, respectively. Importantly, *as iodine is progressively added, the starting phase is diminished while simultaneously a new phase grows in.* By $y \approx 1.1$, the starting structure is no longer evident. At intermediate doping levels ($0 < y \lesssim 1.1$), the starting phase and the doped phase coexist. Furthermore, at these intermediate levels, the observed powder diffraction patterns can be duplicated by the patterns of simple admixtures of the pure $y = 0$ and $y = 1.1$ phases. These observations argue that the doping process is largely if not exclusively heterogeneous for $[Si(Pc)O]_n$ and $[Ge(Pc)O]_n$. The exact structural scale of the inhomogeneity is presently under investigation.

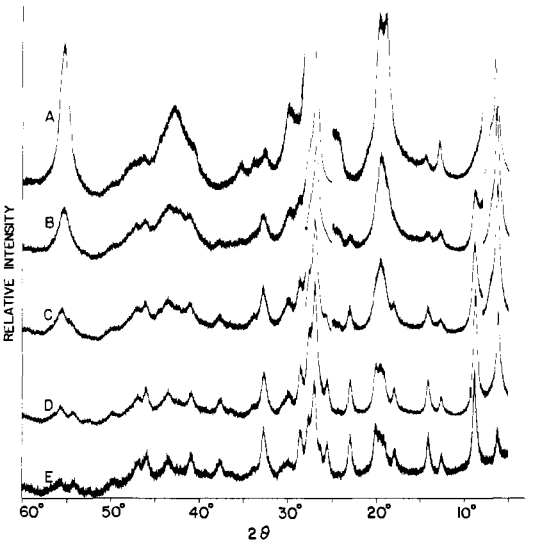

Figure 8. X-ray powder diffractometric study of the progressive doping of $([Si(Pc)O]I_y)_n$ by iodine. (A) $y = 0.0$. Vertical scale: 5–8°, 20 kcps; 8–25°, 2 kcps; 25–28°, 20 kcps; 28–60°, 2 kcps. (B) $y = 0.12$. Vertical scale: 5–8°, 10 kcps; 8–25°, 2 kcps; 25–28°, 8 kcps; 28–60°, 2 kcps. (C) $y = 0.31$. Vertical scale: 5–8°, 4 kcps; 8–25°, 2 kcps; 25–28°, 4 kcps; 28–60°, 2 kcps. (D) $y = 0.71$. Vertical scale: 2 kcps. (E) $y = 1.12$. Vertical scale: 2 kcps.

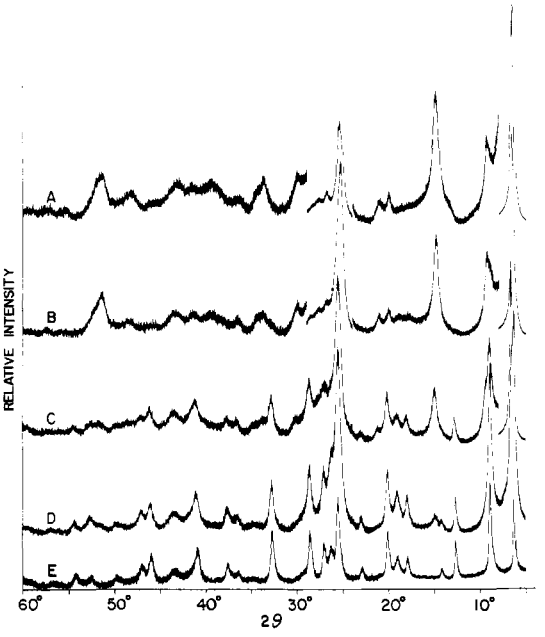

Figure 9. X-ray powder diffractometric study of the progressive doping of $([Ge(Pc)O]I_y)_n$ by iodine. (A) $y = 0.0$. Vertical scale: 5–8°, 20 kcps; 8–24°, 2 kcps; 24–29°, 8 kcps; 29–60°, 2 kcps. (B) $y = 0.10$. Vertical scale: 5–8°, 10 kcps; 8–24°, 2 kcps; 24–29°, 4 kcps; 29–60°, 2 kcps. (C) $y = 0.31$, Vertical scale: 5–8°, 8 kcps; 8–60°, 2 kcps. (D) $y = 0.56$. Vertical scale: 2 kcps (E) $y = 1.12$. Vertical scale: 2 kcps.

Since the infrared and magnetic data suggested considerable chemical complexity, the doping process was not examined in depth

(18) (a) Coates, G. E.; Wade, K. "Organometallic Compounds", 3rd ed.; Methuen: London, 1967; Vol. 1, pp 444–446. (b) Abel, E. W. In "Comprehensive Inorganic Chemistry"; Bailar, J. C., Emeleus, H. J., Nyholm, R., Trotman-Dickenson, A. F., Eds.; Pergamon Press: Oxford, 1973; Vol. 2, pp 69–71. (c) Drake, J. E.; Kasrou, L. N. *Rev. Silicon Germanium, Tin, Lead Compd* **1980**, *4*, 271–367.

(19) (a) Marks, T. J.; Stojakovic, D. R. *J. Am. Chem. Soc.* **1978**, *100*, 1695–1705 and references therein. (b) Schaffer, A. M.; Gouterman, M.; Davidson, E. R. *Theor. Chim. Acta* **1973**, *30*, 9–30. (c) Schaffer, A. M.; Gouterman, M. *Ibid.* **1972**, *25*, 62–82. (d) Edwards, L.; Gouterman, M. *J. Mol. Spectrosc.* **1970**, *33*, 292–310. (e) Chen, I. *Ibid.* **1967**, *23*, 131–143.

(20) (a) Cahill, A. E.; Taube, H. *J. Am. Chem. Soc.* **1951**, *73*, 2847–2851. (b) Dolphin, D.; Forman, A.; Borg, D. C.; Fajer, J.; Felton, R. H. *Proc. Natl. Acad. Sci. U.S.A.* **1971**, *68*, 614–618.

(21) (a) Mizuno, M.; Tanaka, J.; Harada, I. *J. Phys. Chem.* **1981**, *85*, 1789–1794. (b) Gabes, W.; Stufkens, D. J. *Spectrochim. Acta, Part A* **1974**, *30A*, 1835–1841.

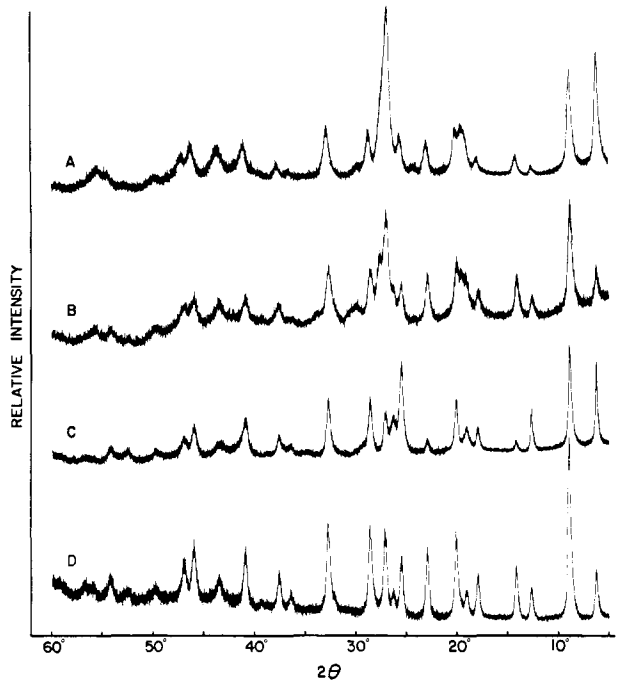

Figure 10. X-ray powder diffractometric traces: (A) $([Si(Pc)O]Br_{1.13})_n$; vertical scale, 2 kcps. (B) $([Si(Pc)O]I_{1.12})_n$; vertical scale, 1 kcps. (C) $([Ge(Pc)O]I_{1.12})_n$; vertical scale, 2 kcps. (D) Ni(Pc)I; vertical scale, 2 kcps.

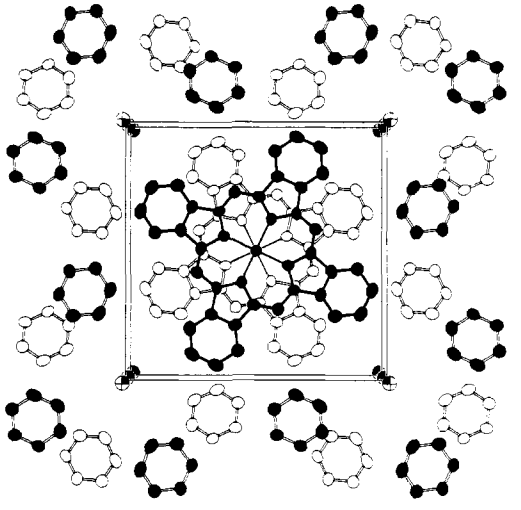

Figure 11. Crystal structure of Ni(Pc)I viewed parallel to the stacking direction. Single-crystal results of ref 3a.

for $[Sn(Pc)O]_n$. Powder diffractograms of heavily doped samples bore no resemblance to those of the $([Si(Pc)O]I_y)_n$ and $([Ge(Pc)O]I_y)_n$ materials.

The structure(s) of the fully doped M = Si and Ge phases were also of interest. In Figure 10 are shown powder diffraction patterns for the bromine- and iodine-doped silicon polymer, the iodine-doped germanium polymer, and Ni(Pc)I. As determined from single-crystal studies,[3a] the latter material crystallizes in the tetragonal crystal system (space group D_{4h}^2-$P4/mcc$, $Z = 2$, $a =$ 13.936 (6) Å, $c = 6.488$ (3) Å) with stacks of staggered (39.5°) $Ni(Pc)^{0.33+}$ units (3.244-Å separation) and chains of disordered I_3^- counterions extending parallel to c. These results are illustrated in Figure 11. It can be seen in Figure 10 that the powder patterns of the four materials are strikingly similar; those of $([Si(Pc)O]Br_{1.13})_n$ and $([Si(Pc)O]I_{1.12})_n$ are nearly identical.

The numerical analysis of the diffraction data for the fully doped silicon and germanium polymers was carried out by using the computer simulation methodology already applied to the undoped materials.[2] $([Si(Pc)O]I_{1.12})_n$ and $([Ge(Pc)O]I_{1.12})_n$ can be

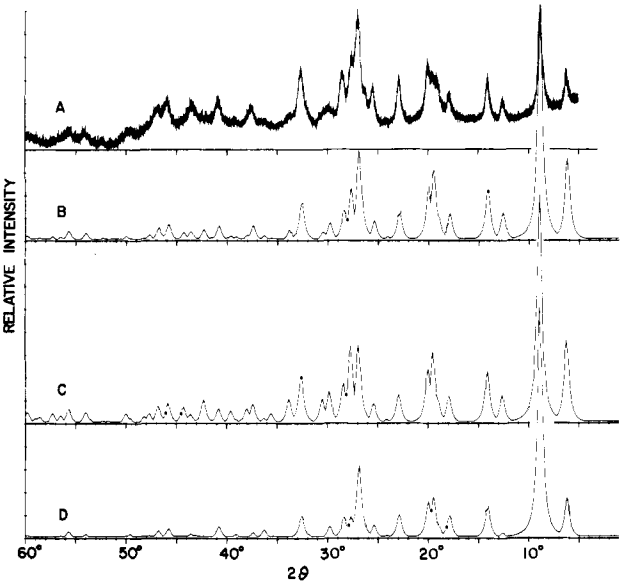

Figure 12. (A) Experimental X-ray diffraction pattern for $([Si(Pc)O]I_{1.12})_n$ (B) Theoretical pattern for the structure given in Table IV with 39.5° staggering of the neighboring phthalocyanine rings and disordered I_3^- ions. (C) Same structure but with ordered I atoms. (D) Same structure but with a 30° staggering angle and disordered I_3^- ions.

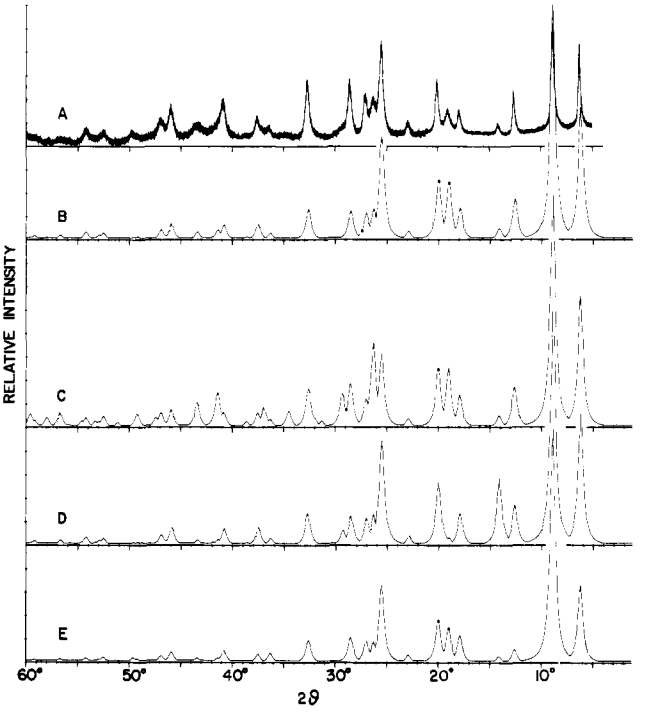

Figure 13. (A) Experimental X-ray diffraction pattern of $([Ge(Pc)O]I_{1.12})_n$. (B) Calculated pattern for the structure given in Table IV with 39.5° staggering of neighboring phthalocyanine rings and disordered I_3^- ions. (C) Same structure but with ordered iodine atoms (see text). (D) Space group $P4/m$, $a = 13.96$ and $c = 3.48$ Å, eclipsed neighboring rings and disordered I_3^- ions. E. Same structure but with a 30° staggering angle and disordered I_3^- ions.

straightforwardly indexed in the tetragonal crystal system, with the reflections for $2\theta < 27°$ giving information principally on the architecture of the metallomacrocyclic stack (Figures 12 and 13), while the larger angle reflections are more sensitive to the halogen positions (vide infra). The slight preferential ordering of the $([Si(Pc)O]I_{1.12})_n$ crystallites (see Experimental Section) did not significantly affect the analysis for this material. The structures are essentially isostructural with Ni(Pc)I, the major differences being the interplanar, ring–ring spacings. In the single-crystal

Table IV. Crystallographic Data for Halogen-Oxidized Phthalocyanine Materials

compd	space group	Z	cell parameters, Å	density, g cm^{-3} calcd	density, g cm^{-3} found	interplanar spacing, Å	staggering angle, deg
Ni(Pc)I[a]	$P4/mcc$	2	a = 13.936 (6), c = 6.488 (3)	1.84	1.78 (4)	3.244 (2)	39.5
$([Si(Pc)O]I_{1.12})_n$	$P4/mcc$	2	a = 13.97 (5), c = 6.60 (4)	1.802 (24)	1.744 (10)	3.30 (2)	39 (3)
$([Si(Pc)O]Br_{1.12})_n$	$P4/mcc$	2	a = 13.97 (5), c = 6.60 (4)			3.30 (2)	39 (3)
$([Ge(Pc)O]I_{1.07})_n$	$P4/mcc$	2	a = 13.96 (5), c = 6.96 (4)	1.805 (23)	1.774 (10)	3.48 (2)	40 (4)

[a] Single-crystal data of ref 3a.

diffraction study of Ni(Pc)I,[3a] the chains of triiodide ions extending parallel to c are disordered with respect to one another.[22] Analysis of diffuse scattering (commensurate supercells consist of three Bragg sites; i.e., the repeat distance is 9.72 Å) data yielded a structural model in which linear I_3^- units (I–I = 3.00 Å) were arrayed at 3.72-Å intermolecular spacings with variability in the c coordinate of +0.245 (2), 0.0, −0.245 (2) Å (there is $^1/_3$ occupancy at each iodine position).

In regard to the diffraction analysis for the $([M(Pc)O]I_y)_n$ materials, it is first of importance to note that the greater interplanar spacings relative to Ni(Pc)I mean that if inter-I_3^- distances are to remain at 3.72 Å, the triiodide lattice can no longer be commensurate (in terms of the aforementioned relationship of 9.72 Å and c) with the M(Pc) lattice and that the M/I ratio can no longer be 1.0; that is, the channels can now accommodate more iodine (a similar situation has been noted for substituting polybromides for polyiodides[14]). Assuming the 3.72-Å spacing, maximum stoichiometries are calculated to be $([Si(Pc)O]I_{1.02})_n$ and $([Ge(Pc)O]I_{1.07})_n$. In regard to the evaluation of various structural models, only a commensurate structure (y = 1.0) could be explicitly tested. For $([Si(Pc)O]I_{1.12})_n$, a hypothetical model with ordered I atoms at 3.30-Å separations produced a detectably poor fit (Figure 12C) as did a Ni(Pc)I model (I atoms disordered over three equally populated sites, separated in this case by required distance of 0.30 Å). Disagreement was particularly evident in the $l \neq 0$ reflections. A model in which the I atoms were distributed over five or more sites centered at z = 0.25 (Figure 12B) gave a more satisfactory fit. Changes in ring conformation (e.g., Figure 12D) are clearly detectable in this model. For $([Ge(Pc)O]I_{1.12})_n$ (Figure 13), satisfactory visual fits could only be obtained for iodine disordered models in which the I atoms were distributed over greater than nine equally populated sites (e.g., fits for ordered I atoms (Figure 13C)), a Ni(Pc)I model, and a $([Si(Pc)O]I_{1.12})_n$ model were less satisfactory.[23a] Again, differentiation between various staggering angles is evident (Figure 13D,E). It is expected that the theoretical pattern for the incommensurate structural model would be similar to those of the other highly disordered structures. In summary, the $([M(Pc)O]I_y)_n$ diffraction analysis is in best agreement with a structural model in which there is considerable disorder in the I_3^- positions along c.

Crystallographic data and calculated vs. experimental density data (which are in good agreement) for the $([M(Pc)O]I_y)_n$ materials are compiled in Table IV. Two important structural features of the metallomacrocyclic stack emerge from the fitting of the theoretical diffraction patterns. First, there appears to be a slight but detectable contraction in the interplanar spacings upon partial oxidation, viz., 0.03 (2) Å, M = Si, and 0.05 (2) Å, M = Ge. A similar observation has been made in several metallobis(glyoximate) systems.[3b,13,23b] Secondly, oxidation induces a change in conformation from eclipsed to staggered in the phthalocyanine rings of $[Ge(Pc)O]_n$.

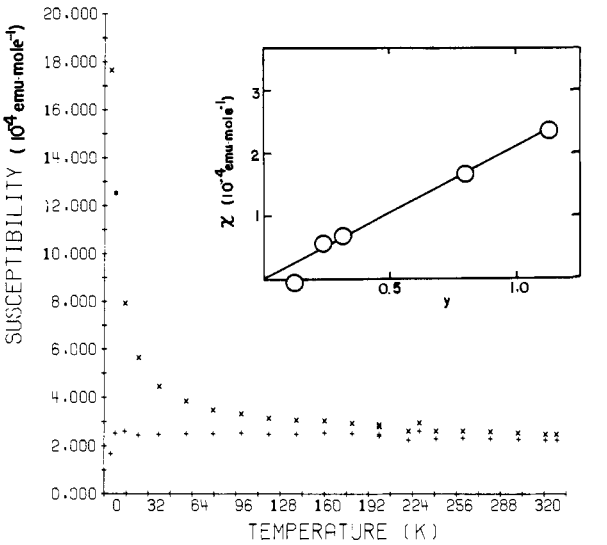

Figure 14. Static magnetic susceptibility of $([Si(Pc)O]I_y)_n$, y = 1.13, as a function of temperature; x, paramagnetic Curie component; +, Pauli-like component. Inset: Pauli-like susceptibility as a function of dopant level, y.

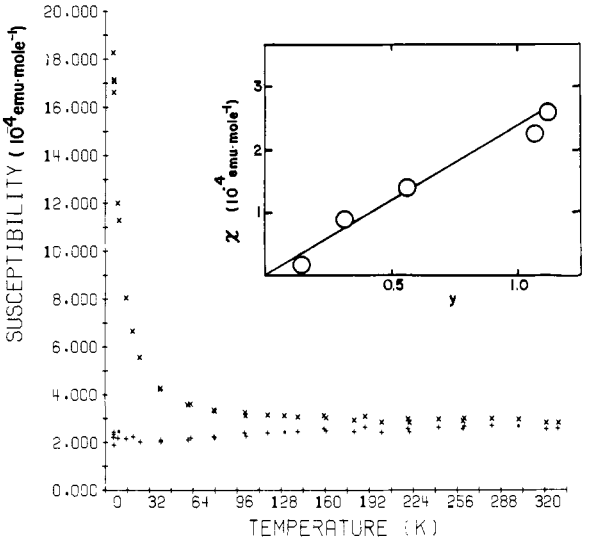

Figure 15. Static magnetic susceptibility of $([Ge(Pc)O]I_y)_n$, y = 1.12, as a function of temperature; x, paramagnetic Curie component; +, Pauli-like component. Inset: Pauli-like susceptibility as a function of dopant level, y.

$([M(Pc)O]I_y)_n$ Magnetism. Static Susceptibility. The magnetic susceptibility of the $([M(Pc)O]I_y)_n$ materials was studied as a function of dopant level and temperature by using a highly sensitive SQUID susceptometer. The diamagnetic corrections ($[M(Pc)O]_n$) to the observed susceptibilities were made by subtracting twice the tabulated (Pascal) Cl contribution and adding the tabulated O contribution to the data for very pure $M(Pc)Cl_2$ samples. This gave results in excellent agreement with those calculated exclusively on the basis of Pascal constants. This procedure was preferred over using measured $[M(Pc)O]_n$ susceptibilities because it could not be ensured that some oxidation had not occurred under

(22) This is a common structural motif for low-dimensional, iodine-oxidized materials.[3b]

(23) (a) Analysis of the Ni(Pc)I powder data evidenced somewhat greater disorder in the triiodide chains than found in the single-crystal study.[3a] It is not unexpected that such factors will be a sensitive function of the crystallization conditions: Khanna, S. K.; Yen, S. P. S.; Somoano, R. B.; Chaikin, P. M.; Ma, C. L.; Williams, R.; Samson, S. *Phys. Rev. B: Condens. Matter* **1979**, *B19*, 655–663. (b) Brown, L. D.; Kalina, D. W.; McClure, M. S.; Shultz, S.; Ruby, S. L.; Ibers, J. A.; Kannewurf, C. R.; Marks, T. J. *J. Am. Chem. Soc.* **1979**, *101*, 2937–2947.

Table V. Magnetic Data for $([M(Pc)O]I_y)_n$ Polymers and Ni(Pc)I

compd	Pauli χ, emu mol^{-1}	spins/M(Pc)	$4t$, eV	interplanar spacing, Å
Ni(Pc)I	$+1.90\ (10) \times 10^{-4}$	0.15 (1)	0.43 (3)	3.244 (2)
$([Si(Pc)O]I_{1.12})_n$	$+2.35\ (11) \times 10^{-4}$	0.18 (1)	0.32 (3)	3.30 (2)
$([Ge(Pc)O]I_{1.12})_n$	$+2.70\ (10) \times 10^{-4}$	0.21 (1)	0.28 (2)	3.48 (2)

the rather drastic polymerization conditions. The diamagnetic correction for I_3^- was calculated as described in the Experimental Section. Typical $([Si(Pc)O]I_y)_n$ and $([Ge(Pc)O]I_y)_n$ susceptibility data are shown in Figures 14 and 15, respectively. Several features are noteworthy. First, all samples exhibited "Curie tailing"[24] at low temperatures. This is a common observation in the magnetic susceptibility of organic conductors and is usually attributed to impurities, defects, or possibly disorder.[24,25] Assuming in the present case localized $S = {}^1/_2$ impurities, linear regression analysis revealed that the actual percentage of this Curie-like species varied from sample to sample and from batch to batch. The percentage was never greater than ca. 2.5% and did not correlate with the level of doping. Subtraction of the Curie component from the measured $([M(Pc)O]I_y)_n$ susceptibilities yielded, for M = Si and Ge, susceptibilities which vary only weakly with temperature, i.e., which are nearly Pauli-like (Figures 14 and 15).[4,26] Such behavior is reminiscent of Ni(Pc)I[3a,27] but is atypical of most low-dimensional conductive materials.[3b,4] Importantly, the Pauli-like component of the susceptibility in the present case correlates *linearly* with the doping level (see insets in Figures 13 and 14), having zero intercept at zero doping. This is consistent with other evidence (vide infra) that the doping is largely heterogeneous; that is, a single, discrete phase with Pauli-like susceptibility is created as iodine is incrementally added. The foregoing spectroscopic evidence and X-ray data previously discussed indicate that this phase possesses a Ni(Pc)I-type structure with $y \approx 1.1$.

In marked contrast to the Si and Ge systems but perhaps not unexpected on the basis of the infrared spectroscopic results, the magnetic behavior of the $([Sn(Pc)O]I_y)_n$ materials was less straightforward. Both the Curie and non-Curie parts of the paramagnetism are comparatively low. Thus, the former was always less than 1.7%, while the latter never exceeded ca. 1×10^{-4} emu mol^{-1} and did not depend on the dopant level. This suggests that the bulk of the M = Sn iodination products are diamagnetic.

Magnetic data for the $([Si(Pc)O]I_{1.12})_n$ and $([Ge(Pc)O]I_{1.12})_n$ polymers are set out in Table V. It can be seen that the room-temperature Pauli-like susceptibilities are close to that found for Ni(Pc)I,[3a,27] as are calculated[28] unpaired spins (assuming $S = {}^1/_2$, $g = 2.00$) per M(Pc) unit. Making the simplistic but pragmatic working assumption of a one-dimensional, tight-binding band description with noninteracting electrons (the Hubbard on-site Coulomb repulsion integral $U = 0$), a Pauli susceptibility (at 0 K) can be expressed as in eq 2,[24b,29] where N is Avogadro's number,

$$\chi^P = \frac{N\mu_B^2}{t\pi \sin(\pi\rho/2)} \qquad (2)$$

μ_B is the Bohr magneton, t is the transfer (resonance) integral (bandwidth/4), and ρ is the degree of partial oxidation.[30] The derived "magnetic" bandwidths (Table V) are in the general range (perhaps the low end—vide infra) found for other low-dimensional organic molecular conductors[4] and, in the present case, inversely parallel the interplanar, ring–ring spacings. The measured unpaired spins per M(Pc) roughly parallel the interplanar spacings.

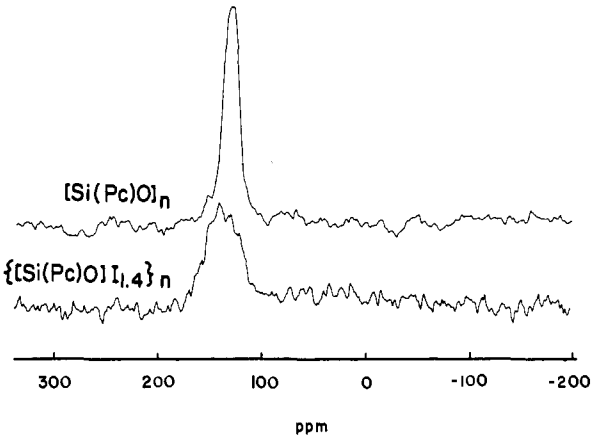

Figure 16. High-resolution 15-MHz solid-state ^{13}C NMR spectra of doped and undoped $[Si(Pc)O]_n$. Parameters: ^1H pulse width = 5.5 μs, contact time = 3.0 ms, pulse delay = 5.0 s.

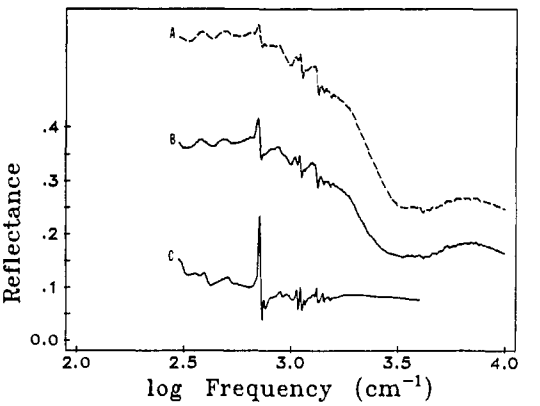

Figure 17. Optical reflectance spectra of polycrystalline $([Si(Pc)O]I_y)_n$ samples: (A) $y = 0.71$; (B) $y = 0.31$; (C) $y = 0.00$. Successive plots (C → A) are displaced vertically by +0.10 reflectance units.

$([Si(Pc)O]I_y)_n$ Solid-State ^{13}C NMR Spectroscopy. High-resolution carbon NMR spectroscopy acquired with cross-polarization (CP) and magic angle spinning (MAS) has proven to be a powerful structural tool for polymers in the solid state.[31] Recently it has also been applied to the study of electrically conductive polymers, since in principle it could provide information on the doping process and nuclear-conduction electron interactions.[32] The ^{13}C CP-MAS spectra of all of the $[M(Pc)O]_n$

(24) (a) Scott, J. C.; Garito, A. F.; Heeger, A. J. *Phys. Rev. B: Condens. Matter* **1974**, *B10*, 3131–3139. (b) Isett, L. C. *Ibid.* **1978**, *B18*, 439–447. (c) Delhaes, P.; Coulon, C.; Flandrois, S.; Hilti, B.; Mayer, C. W.; Rihs, G.; Rivory, J. *J. Chem. Phys.* **1980**, *73*, 1452–1463.

(25) (a) Bailey, J. C.; Chesnut, D. B. *J. Chem. Phys.* **1969**, *51*, 5118–5128. (b) Bulaevskii, L. N.; Zvarykina, A. V.; Karimov, Yu. S.; Lyubovskii, R. B.; Shchegolev, I. F. *JETP (Engl. Transl.)* **1972**, *35*, 384–389. (c) Azevedo, L. J.; Clark, W. G. *Phys. Rev. B: Condens. Matter* **1977**, *B16*, 3252–3258.

(26) Kittel, C. "Introduction to Solid State Physics", 5th ed.; Wiley: New York, 1976; Chapter 14.

(27) We have now remeasured the magnetic susceptibilities of Ni(Pc) and Ni(Pc)I using the more sensitive SQUID apparatus. These improved data, which are in good agreement with the EPR data of ref 3a, are given in Table V.

(28) Calculated from the simple Curie relationship[26]

$$\chi = \frac{Ng^2\mu_B^2 S(S+1)}{3kT}$$

(29) (a) Shiba, H. *Phys. Rev. B: Condens. Matter* **1972**, *B6*, 930–938. (b) Torrance, J. B.; Tomkiewicz, Y.; Silverman, B. D. *Ibid.* **1977**, *B15*, 4738–4749.

(30) Taken to be $y/3$ for the fully doped polymers.

(31) (a) Schaefer, J. *Top. C-13 NMR Spectrosc.* **1979**, *3*, 284–321. (b) Vaughan, R. W. *Annu. Rev. Phys. Chem.* **1978**, *29*, 397–419. (c) Yannoni, C. S. *Acc. Chem. Res.* **1982**, *15*, 201–208 and references therein.

(32) (a) Clarke, T. C.; Scott, J. C.; Yannoni, C. S. *Polym. Prepr., Am. Chem. Soc., Div. Polym. Chem.* **1982**, *23*, 77–78. (b) Peo, M.; Förster, H.; Menke, K.; Hocker, J.; Gardner, J. A.; Roth, S.; Dransfeld, K. *Solid State Commun.* **1981**, *38*, 467–468. (c) Peo, M.; Förster, H.; Menke, K.; Hocker, J.; Gardner, J. A.; Roth, S.; Dransfeld, K. *Mol. Cryst. Liq. Cryst.* **1981**, *77*, 103–110. (d) Gibson, H. W.; Pochan, J. M.; Kaplan, S. *J. Am. Chem. Soc.* **1981**, *103*, 4619–4620. (e) Dirk, C. W.; Marks, T. J., manuscript in preparation. (f) Maricq, M. M.; Waugh, J. S.; MacDiarmid, A. G.; Shirakawa, H.; Heeger, A. J. *J. Am. Chem. Soc.* **1978**, *100*, 7729–7730.

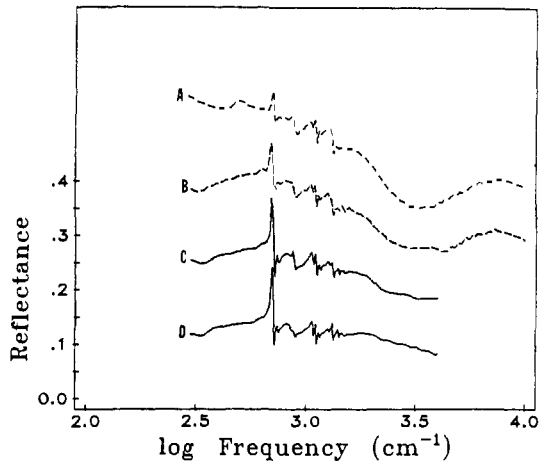

Figure 18. Optical reflectance spectra of polycrystalline $([Ge(Pc)O]I_y)_n$ samples: (A) $y = 1.07$; (B) $y = 0.56$; (C) $y = 0.31$; (D) $y = 0.0$; successive plots (D → A) are displaced vertically by +0.10 reflectance units.

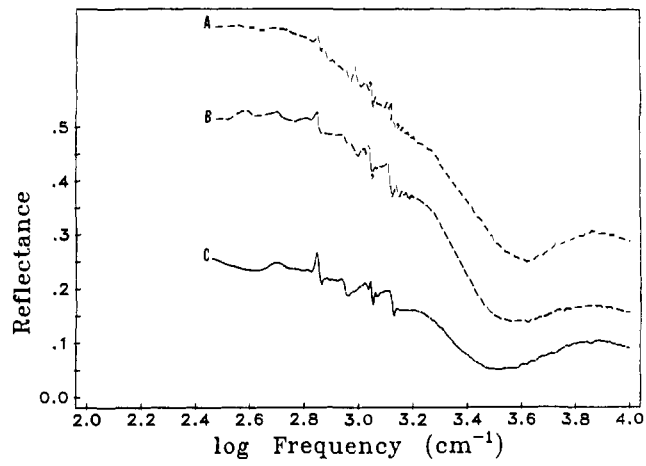

Figure 19. Optical reflectance spectra of polycrystalline samples: (A) Ni(Pc)I; (B) $([Si(Pc)O]I_{1.12})_n$; (C) $([Ge(Pc)O]I_{1.12})_n$. Successive plots (C → A) are displaced vertically by +0.10 reflectance units.

materials exhibit a multiplet in the 130-ppm (vs. Me_4Si) region. The chemical shift dispersion is only slightly better resolved at 50.0 MHz than at 15.1 MHz. This spectral region is that expected for aromatic, phthalocyanine carbon resonances.[32e,33] Upon doping $[Si(Pc)O]_n$ (Figure 16), the line broadens and shifts ca. 10 ppm to lower field. Resolution was insufficient to unambiguously indicate whether doping was homogeneous or inhomogeneous. There is no evidence for the formation of sp^3 carbon atoms. The direction and magnitude of the shift upon doping are similar to those reported for other acceptor-doped polymers.[32] As noted previously,[32a] this behavior can be explained by the carbonium ion character of the oxidized state without invoking a significant Knight shift. In ^{13}CN-enriched TTF–TCNQ, an upfield shift of 300–400 ppm is observed upon formation of the mixed-valent complex.[34]

$([M(Pc)O]I_y)_n$ Optical Reflectivity. Optical reflectance studies, interpreted within the framework of simple free electron models, have provided useful information on the electronic structure and transport characteristics of low-dimensional molecular materials[4,35] as well as electroactive polymers.[6,35a,36] The broad infrared absorption already noted in transmission spectra (vide supra) prompted further investigations of $([M(Pc)O]I_y)_n$ optical characteristics by reflectance as a function of M and y. Samples were studied as compressed polycrystalline pellets (identical with those employed for diffraction and conductivity studies) over frequency ranges as large as 100–50 000 cm^{-1}, and data were processed by using numerical techniques described elsewhere.[7a] Beginning with $[Si(Pc)O]_n$ (Figure 17), it can be seen that progressive doping with I_2 results in the appearance of a plasma-like edge (by $y \approx 0.30$) with a reflectivity minimum in the vicinty of ca. 3600 cm^{-1}. This feature can be correlated with the changes upon doping already noted in the transmission infrared spectra (vide supra); similar effects are observed upon doping polyacetylene with acceptors.[36] Also evident in Figure 17 is a diminution upon doping of the sharp molecular mode at 700 cm^{-1} and the possible growth and/or enhancement of sharp modes at ca. 400, 450, 1100, and 1260 cm^{-1}. These latter features are of course indicative of electron–phonon coupling effects.[4] Progressive doping of $[Ge(Pc)O]_n$ also results in the appearance of a plasma-like feature (Figure 18) and a reflectivity minimum at slightly lower frequency than in the silicon analogue, ca. 3200 cm^{-1}. For the germanium system, higher doping levels are required before the plasma-like edge is visible, and the ultimate low-energy reflectance is lower than for silicon. Some of this effect is no doubt due to the slightly greater preferential orientation of the c direction of the $([Si(Pc)O]I_{1.12})_n$ crystallites in the plane perpendicular to the propagating radiation (see Experimental Section). This would enhance reflectance since this band-related transition is expected[35] to be polarized in the chain (stacking) direction. It will be seen that Ni(Pc)I (vide infra), which exhibits higher preferential orientation, shows this effect more strongly, as expected. As in the case of the $[Si(Pc)O]_n$ system, doping also results in a diminution of the M(Pc) molecular mode at 700 cm^{-1}. Again, features at ca. 1100 and 1260 cm^{-1} are visible in the highest doped material.

The reflectance spectrum of Ni(Pc)I is shown in Figure 19 and compared to those of $([Si(Pc)O]I_{1.12})_n$ and $([Ge(Pc)O]I_{1.12})_n$. The nickel compound also exhibits a plasma-like feature and a reflectivity minimum at ca. 4200 cm^{-1}—the highest energy for the three face-to-face phthalocyanine arrays. The low-energy reflectivity of the nickel compound is higher than for the silicon and germanium polymers, in accord with the higher percentage of phthalocyanine stacks oriented perpendicular to the direction of light propagation and the expected polarization of the plasmon transition. The molecular mode structure in the reflectance spectrum of Ni(Pc)I is similar to that in the silicon and germanium systems, in accord with the ligand-centered nature of conduction band electronic structure; that is, these are predominantly phthalocyanine skeletal modes.

An analysis of *isotropic* reflectance data for low-dimensional materials is necessarily approximate. However, in view of previous correlations that have been drawn between isotropic and single-crystal data,[35h,d,h] the close structural similarities among the present materials, and the diffraction-derived information available on crystallite orientations in these materials, it is reasonable to investigate qualitative, comparative trends. The present reflectance data analysis began with a correction for the largely but not entirely isotropic character of the crystallite orientations using methods described previously.[35h] Next, the corrected data were fit by nonlinear least-squares techniques[6a,37a] to a simple Drude

(33) (a) Janson, T. F.; Katz, J. J. *Porphyrins* **1979**, *4*, 1–59. (b) Johnson, L. F.; Jankowski, W. C. "Carbon-13 NMR Spectra", Wiley-Interscience: New York, 1972.

(34) Rybaczewski, E. F.; Smith, L. S.; Garito, A. F.; Heeger, A. J.; Silbernagel, B. G. *Phys. Rev. B: Condens. Matter* **1976**, *B14*, 2746–2756.

(35) (a) Tanner, D. B. in ref 4a; Vol. 2, pp 205–258. (b) Madison, M. R.; Coleman, L. B.; Somoano, R. B. *Solid State Commun.* **1981**, *40*, 979–982. (c) Weinstein, B. A.; Slade, M. L.; Epstein, A. J.; Miller, J. S. *Ibid.* **1981**, *37*, 643–646 and referneces therein. (d) Torrance, J. B.; Scott, B. A.; Welber, B.; Kaufman, F. B.; Seiden, P. E. *Phys. Rev. B: Condens. Matter* **1979**, *B19*, 730–741. (e) Delhaes, P.; Coulon, C.; Amiell, J.; Flandrois, S.; Toreilles, E.; Fabre, J. M.; Giral, L. *Mol. Cryst. Liq. Cryst.* **1979**, *50*, 43–58. (f) Jacobsen, C. S.; Mortensen, K.; Andersen, J. R.; Bechgaard, K. *Phys. Rev. B: Condens. Matter* **1978**, *B18*, 905–921. (g) Somoano, R. B.; Yen, S. P. S.; Hadek, V.; Khanna, S. K.; Novotny, M.; Datta, T.; Hermann, A. M.; Woollam, J. A. *Ibid.* **1978**, *B17*, 2853–2857. (h) Bright, A. A.; Garito, A. F.; Heeger, A. J. *Phys. Rev.*, **1974**, *10*, 1328–1342.

(36) (a) Etemad, S.; Heeger, A. J.; Lauchlan, L.; Chung, T.-C.; MacDiarmid, A. G. *Mol. Cryst. Liq. Cryst.* **1981**, *77*, 43–63. (b) Fincher, C. R., Jr.; Ozaki, M.; Tanaka, M.; Peebles, D.; Lauchlan, L.; Heeger, A. J.; MacDiarmid, A. G. *Phys. Rev. B: Condens. Matter* **1979**, *B20*, 1589–1602.

(electron gas) model for the dielectric function $\epsilon(\omega)$ (eq 3). Here

$$\epsilon(\omega) = \epsilon_{core} - \frac{\omega_p^2}{\omega^2 + i\omega/\tau} \quad (3)$$

ϵ_{core} is the dielectric constant arising from the core polarizability, τ is the electronic relaxation time (scattering of electrons near the Fermi surface), and ω_p is the plasma frequency.[37b] The relationship between ω_p and the carrier density per unit volume,[37c] N_c, and the optical effective mass of the carriers, m^*, is given by eq 4. The present fitting procedure yielded the ϵ_{core}, ω_p, and τ

$$\omega_p^2 = 4\pi N_c e^2/m^* \quad (4)$$

values set out in Table VI. From the plasma frequency, it is possible to obtain approximate, comparative bandwidth information in the stacking direction if a simple, one-dimensional tight-binding band is assumed (eq 5) (as was done in the discussion

$$4t = \frac{17.4\rho(h\omega_p)^2}{N_c c^2 \sin(\pi\rho/2)} \quad (5)$$

of the magnetic data). Here ρ is the degree of partial oxidation and c is the interplanar spacing. Calculated bandwidths for Ni(Pc)I, $([Si(Pc)O]I_{1.12})_n$, and $([Ge(Pc)O]I_{1.12})_n$ are compiled in Table VI. The relative effects of the interplanar spacing are clearly evident, and the calculated bandwidths are in reasonable agreement with those obtained from the magnetic susceptibility measurements, considering the approximations used. Equally important, the parameters derived from the Drude fit are in the range derived in similar analyses for other low-dimensional organic molecular conductors.[4,35,38] It was also possible to calculate the effective masses of the carriers from eq 4, and optically derived estimates of the DC conductivities from eq 6. These parameters

$$\sigma_{opt} = \omega_p^2\tau/4\pi \quad (6)$$

are also set out in Table VI. It will be seen that the conductivities are of approximately the correct order of magnitude for charge transport in the phthalocyanine stacking direction (vide infra). The effective carrier masses are in the range found for other low-dimensional conductors.[4,35] Variable-temperature studies as well as further measurements in the far-infrared are in progress.

$([M(Pc)O]X_y)_n$ Charge Transport. DC electrical conductivity measurements on the halogen-doped cofacial phthalocyaninato polymers were performed in the four-probe geometry, using compressed polycrystalline samples (pellets identical with those used for diffraction and reflectance studies). Although measurements on this form of sample are obviously not as desirable for a low-dimensional material as those on large, well-formed single crystals (compaction measurements reflect averaging over all crystallographic orientations and interparticle contact resistance), considerable information can still be obtained. This should be especially true of samples with similar chemical compositions, molecular and crystal structures, and in which crystallite orientation is known. A large body of empirical observations[3,4,12c,39] indicates that single-crystal conductivities of low-dimensional materials are typically 10^2–10^3 greater along the molecular stacking axis than as measured for compressed, polycrystalline samples. This approximate correlation is verified by the conductivity data on Ni(Pc)I,[3a] a material closely analogous to the $([M(Pc)O]I_y)_n$ polymers. Furthermore, single-crystal conductivity data are not presently available for any highly conductive, doped organic polymer (data are available, however, for partially oriented samples[41a]).

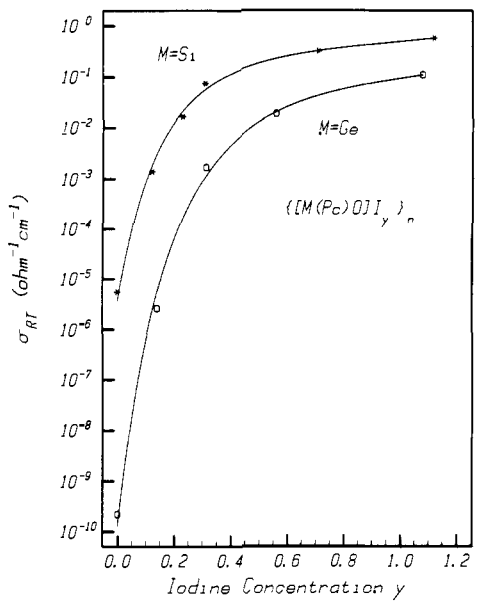

Figure 20. Electrical conductivity vs. dopant level for polycrystalline samples of $([Si(Pc)O]I_y)_n$ and $([Ge(Pc)O]I_y)_n$. The lines through the data points are drawn as a guide to the eye.

Upon incremental doping with iodine, both $[Si(Pc)O]_n$ and $[Ge(Pc)O]_n$ exhibit abrupt increases in electrical conductivity (Figure 20). Conductivity data for the various stoichiometries of iodine doping are set out in Table VII. It can be seen that transport values for bromine-doped materials are closely comparable. In addition to the other physical data presented, this similarity argues, as elaborated fully elsewhere,[12c,14,40] that the polyhalide chains are not a major carrier of charge in these materials.

A similar, abrupt rise in electrical conductivity upon incremental doping has also been observed in polyacetylene, *p*-polyphenylene, and several other conductive polymers. The form of the σ vs. y curve has been variously attributed to a semiconductor–metal transition with either homogeneous or inhomogeneous doping[6c,41,42]

(37) (a)

$$R = \frac{1 + |\epsilon| - [2(|\epsilon| + \epsilon_1)]^{1/2}}{1 + |\epsilon| + [2(|\epsilon| + \epsilon_1)]^{1/2}}$$

where $|\epsilon| = (\epsilon_1^2 + \epsilon_2^2)^{1/2}$. (b) Fitting was carried out between the onset of major molecular features in the low energy portions of the spectra to beyond the reflectivity minima on the high energy side. Variation of these end points by up to a maximum of ca. 500 cm^{-1} generally resulted in ϵ_∞, ω_p, and τ changes of less than 10%. The parameters in Table VI are taken from the middle of this range. (c) Assumed to be holes on the basis of analogous compounds,[4] as well as Hall effect and thermopower data: Lyding, J. W.; Kannewurf, C. R.; Marks, T. J., unpublished results. Values for N_c were calculated from degree of partial oxidation and crystallographic data.

(38) (a) Representative bandwidth results for molecular metals and method of determination: $TTFBr_{0.79}$, 1.13 eV (optical);[35c] $TSeTI_{0.50}$, 0.60 eV (magnetic),[24c] 0.88 eV (optical);[24c] TTT_2I_3, 1.5 eV (optical),[35e] 0.70 eV (thermopower),[38b,c] 0.64 eV (magnetic);[24b] $TTF(SeCN)_{0.58}$, 1.94 eV (thermopower),[38d] 1.22 eV (optical);[35c,38d] 0.43 eV (magnetic);[38e] TTF–TCNQ, ca. 0.5 eV (TCNQ),[38f] ca. 0.25 eV (TTF).[38f] In general, bandwidths are significantly higher in cases with eclipsed (C_n) rather than slipped stacks.[38g] (b) Khanna, S. K.; Yen, S. P. S.; Somoano, R. B.; Chaikin, P. M.; Ma, C. L.; Williams, R.; Samson, S. *Phys. Rev. B: Condens. Matter* **1979**, *B19*, 655–663. (c) Chaikin, P. M.; Grüner, G.; Shchegolev, I. F.; Yagubskii, E. B. *Solid State Commun.* **1979**, *32*, 1211–1214. (d) Somoano, R. B.; Gupta, A.; Hadek, V.; Novotny, M.; Jones, M.; Datta, T.; Deck, R.; Hermann, A. M. *Phys. Rev. B: Condens. Matter* **1977**, *B15*, 595–601. (e) Wudl, F.; Schafer, D. E.; Walsh, W. M., Jr.; Rupp, L. W.; DiSalvo, F. J.; Woszczak, J. V.; Kaplan, M. L.; Thomas, G. A. *J. Chem. Phys.* **1977**, *66*, 377–385. (f) Conwell, E. M. *Phys. Rev. B: Condens. Matter* **1980**, *B22*, 1761–1780 and references therein. (g) Salahub, D. R.; Messmer, R. P.; Herman, F. *Ibid.* **1976**, *B13*, 4252–4257.

(39) (a) Chiang, C. K.; Druy, M. A.; Gau, S. C.; Heeger, A. J.; Louis, E. J.; MacDiarmid, A. G. *J. Am. Chem. Soc.* **1978**, *100*, 1013–1015. (b) Chiang, C. K.; Park, Y. W.; Heeger, A. J.; Shirakawa, H.; Louis, E. J.; MacDiarmid, A. G. *J. Chem. Phys.* **1978**, *69*, 5098–5104. (c) Farges, J. P.; Brau, A.; Gutmann, F. *J. Phys. Chem. Solids* **1972**, *33*, 1723–1726.

(40) (a) Kámaras, K.; Mihály, G.; Grüner, G.; Jánossy, A. *J. Chem. Soc., Chem. Commun.* **1978**, 974–975. (b) Kámaras, K.; Kertesz, M. *Solid State Commun.* **1978**, *28*, 607–611.

(41) (a) Park, Y.-W.; Heeger, A. J.; Druy, M. A.; MacDiarmid, A. G. *J. Chem. Phys.* **1980**, *73*, 946–957 and referneces therein. (b) MacDiarmid, A. G.; Heeger, A. J. in ref 4d; pp 161–186; ref 4b; pp 353–402. (c) Shacklett, L. W.; Chance, R. R.; Ivory, D. M.; Miller, G. G.; Baughman, R. H. *Synth. Met.* **1979**, *1*, 307–320. (d) Chance, R. R.; Shacklette, L. W.; Eckhardt, H.; Sowa, J. M.; Elsenbaumer, R. L.; Ivory, D. M.; Miller, G. G.; Baughman, R. H. in ref 4b; pp 125–135. (e) Rubner, M.; Georger, J., Jr.; Sichel, E. *Polym. Prepr., Am. Chem. Soc., Div. Polym. Chem.* **1982**, *23*, 96–97. (f) Pochan, J. M.; Pochan, D. F.; Rommelmann, H.; Gibson, H. W. *Macromolecules* **1981**, *14*, 110–114 and references therein.

Table VI. Optical Reflectance Data for $([M(Pc)O]I_y)_n$ Polymers and Ni(Pc)I[a]

compd	ω_p, eV	τ, 10^{-15} s	ϵ_{core}	$4t$, eV	m^*/m_0[b]	σ_{opt},[c] Ω^{-1} cm^{-1}
Ni(Pc)I	0.698 (7)	3.78 (4)	3.43 (7)	0.99 (9)	1.5 (2)	400
$([Si(Pc)O]I_{1.12})_n$	0.563 (8)	5.89 (9)	2.78 (7)	0.60 (6)	2.5 (3)	400
$([Ge(Pc)O]I_{1.12})_n$	0.522 (6)	3.97 (10)	2.95 (7)	0.48 (5)	2.9 (3)	200

[a] Standard deviations established via the fitting procedure. [b] m_0 = free electron mass. [c] Calculated from eq 6.

Table VII. Pressed-Powder Electrical Conductivity Data for $([M(Pc)O]X_y)_n$ Doped Polymers at Room Temperature

compd	σ_{RT},[b] Ω^{-1} cm^{-1}	activation energy,[b] eV: low temp	activation energy,[b] eV: high temp
$[Si(Pc)O]_n$	5.5×10^{-6}		0.29
$([Si(Pc)O]I_{0.12})_n$	1.4×10^{-3}	0.078	0.12
$([Si(Pc)O]I_{0.23})_n$	1.7×10^{-2}	0.031	0.058
$([Si(Pc)O]I_{0.31})_n$	7.6×10^{-2}	0.015	0.039
$([Si(Pc)O]I_{0.71})_n$	3.2×10^{-1}	0.011	0.033
$([Si(Pc)O]I_{1.12})_n$	5.8×10^{-1}	0.0071	0.026
$([Si(Pc)O]I_{1.13})_n$	6.7×10^{-1}	0.0089	0.028
$([Si(Pc)O]I_{1.55})_n$	1.4		0.035
$([Si(Pc)O]Br_{1.8})_n$	7.2×10^{-1}	0.020	0.039
$([Si(Pc)O]Br_{1.12})_n$	9.5×10^{-1}	0.0084	0.022
$[Ge(Pc)O]_n$	2.2×10^{-10}		
$([Ge(Pc)O]I_{0.14})_n$	2.6×10^{-6}	0.16	0.19
$([Ge(Pc)O]I_{0.31})_n$	1.7×10^{-3}	0.055	0.078
$([Ge(Pc)O]I_{0.56})_n$	1.9×10^{-2}	0.041	0.057
$([Ge(Pc)O]I_{1.08})_n$	1.1×10^{-1}	0.034	0.042
$[Sn(Pc)O]_n$	1.2×10^{-9}		0.56
$([Sn(Pc)O]I_{0.14})_n$	5.2×10^{-9}	0.30	0.68
$([Sn(Pc)O]I_{0.32})_n$	5.2×10^{-9}	0.59	0.75
$([Sn(Pc)O]I_{0.60})_n$	2.2×10^{-8}	1.19	0.64
$([Sn(Pc)O]I_{1.11})_n$	2.2×10^{-8}	1.08	0.89
$([Sn(Pc)O]I_{1.76})_n$	6.5×10^{-7}	0.76	1.28

[a] Measured by four-probe techniques. [b] Calculated by least-squares fit to eq 9.

or to percolation between highly conductive particles in a poorly conductive medium (also inhomogeneous doping).[4c,42] Since the present case is the only reported example where it is known unambiguously that such behavior arises from inhomogeneous doping involving two polymer phases of well-defined stoichiometry and structure, it was of interest to determine whether the behavior conformed to a simple percolation model[6c,43] for conduction in inhomogeneous media. For a randomly dispersed mixture of conductive and nonconductive particles having roughly similar sizes and shapes, percolation theory for three-dimensions predicts the conductivity dependence shown in eq 7 for the composition

$$\sigma = \sigma_0(X - X_c)^s \quad (7)$$

region near and above the insulator-to-conductor transition threshold. Here, X is the volume fraction of conducting species and X_c is the percolation threshold below which the conductivity falls precipitously. For a three-dimensional continuous random system, X_c is usually near ca. 0.15. However, it is critically dependent upon the dimensionality of the system (two or three), the relative sizes of the particles, the degree of dispersion, and other structural factors. In more extreme cases, values significantly lower than and greater than 0.15 have been observed.[44] Both

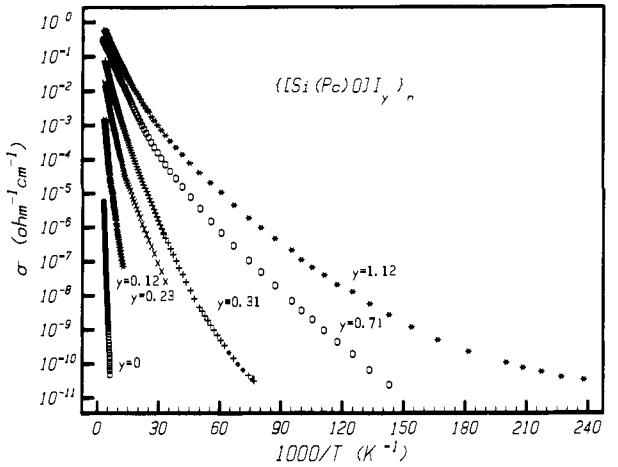

Figure 21. Variable-temperature electrical conductivity data for polycrystalline $([Si(Pc)O]I_y)_n$ samples at various doping levels.

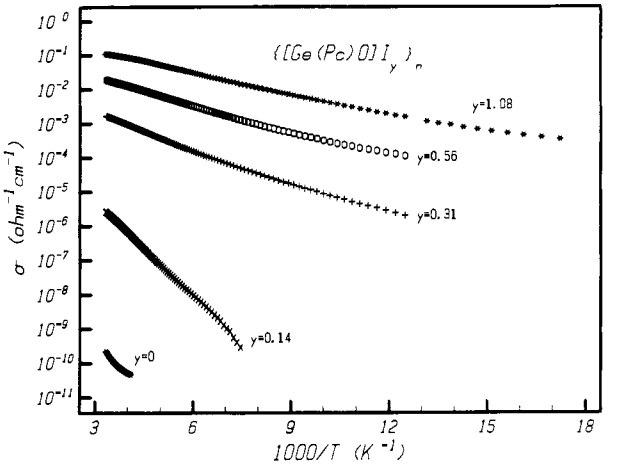

Figure 22. Variable-temperature electrical conductivity data for polycrystalline $([Ge(Pc)O]I_y)_n$ samples at various doping levels.

theory and experiment predict that the exponent s should fall near 1.5–1.7 for a three-dimensional system of randomly dispersed particles. It was found that the σ vs. y data for $([Si(Pc)O]I_y)_n$ could be readily fit to eq 7 by nonlinear regression techniques. The parameters obtained from the fit were $X_c = 0.09$ (1), $s = 1.8$ (2), and $\sigma_0 = 0.65$ (7) Ω^{-1} cm^{-1}. These results are in good accord with a simple percolation model for the dopant-dependent charge-transport behavior in the phthalocyaninato face-to-face polymers. Insufficient data were available to perform a similar analysis on the germanium system.

Variable-temperature conductivity data for the $([Si(Pc)O]I_y)_n$ and $([Ge(Pc)O]I_y)_n$ materials are presented in Figures 21–23. The data for the fully doped materials are compared to data for a polycrystalline compaction of Ni(Pc)I in Figure 23. Owing to diffractometric evidence (see Experimental Section for details) of slight preferential crystallite orientation in the pressed pellets of Ni(Pc)I and $([Si(Pc)O]I_y)_n$, efforts were made to ascertain whether measured conductivities reflected these effects. Four-probe measurements on the different pellet faces, both parallel to and perpendicular to the direction of preferential orientation, revealed that the influence of the preferential orientation on the measured charge transport in any particular direction was no

(42) (a) Epstein, A. J.; Rommelmann, H.; Abkowitz, M.; Gibson, H. W. *Mol. Cryst. Liq. Cryst.* **1981**, *77*, 81–96 and references therein. (b) Enkelmann, V.; Lieser, G.; Monkenbusch, M.; Muller, W.; Wegner, G. *Ibid.* **1981**, *77*, 111–123. (c) Stamm, M.; Hocker, J.; Axmann, A. *Ibid.* **1981**, *77*, 125–135.

(43) (a) Kirkpatrick, S. *Rev. Mod. Phys.* **1973**, *45*, 574–588 and references therein. (b) Seager, C. H.; Pike, G. E. *Phys. Rev. B: Condens. Matter* **1974**, *B10*, 1435–1446 and references therein. (c) Hsu, W. Y.; Barkley, J. R.; Meakin, P. *Macromolecules* **1980**, *13*, 198–200. (d) Lagues, M.; Sauterey, C. *J. Phys. Chem.* **1980**, *84*, 3503–3508.

(44) (a) Clarke, P. S.; Orton, J. W.; Guest, A. J. *Phys. Rev. B: Condens. Matter* **1978**, *B18*, 1813–1817 and data cited therein. (b) Malliaris, A.; Turner, D. T. *J. Appl. Phys.* **1971**, *42*, 614–618.

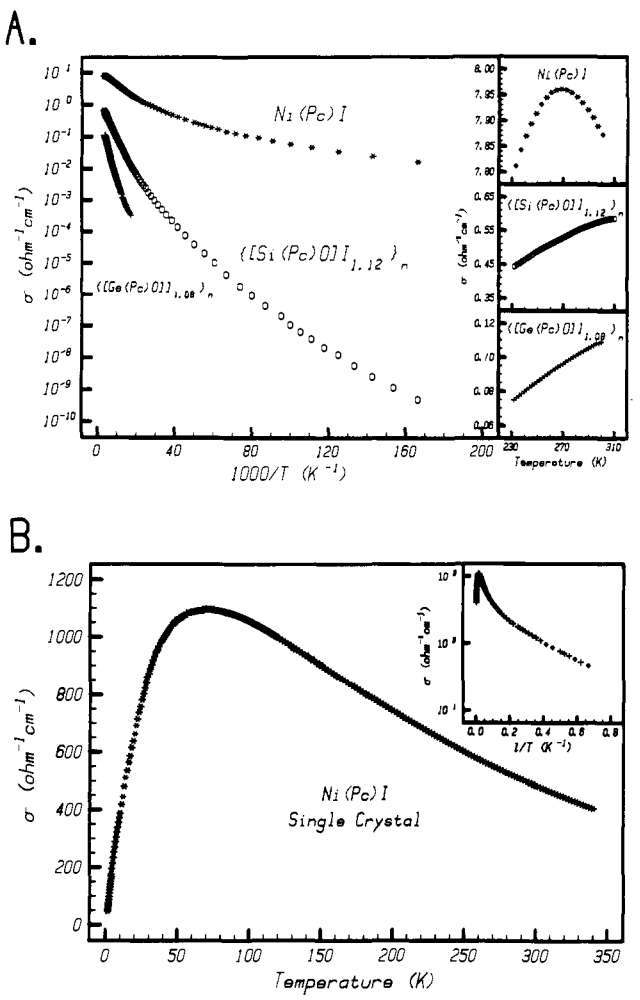

Figure 23. (A) Variable-temperature electrical conductivity data for pressed powder samples of Ni(Pc)I, $\{[Si(Pc)O]I_{1.12}\}_n$, and $\{[Ge(Pc)O]I_{1.08}\}_n$. (B) Variable-temperature conductivity of a typical[3d] Ni(Pc)I single crystal presented here for comparative purposes. The inset illustrates the transition to an activated nonmetallic state at low temperatures, reminiscent of TTT_2I_3.[3b]

greater than the range of conductivities typically measured for different pellets of the same sample. It can be seen that room-temperature conductivities inversely parallel the measured interplanar ring–ring spacings, i.e., $\sigma_{Ni} > \sigma_{Si} > \sigma_{Ge}$. Focusing on the highest temperature portions of the data, it can be seen that the behavior of the nickel powder is distinctly "metal-like" ($d\sigma/dt < 0$) above ca. 270 K (inset, Figure 23A). Of course, typical[3a,d] single crystals of Ni(Pc)I are even more "metal-like" with σ = ca. 250–650 Ω^{-1} cm^{-1} near room temperature and exhibiting a $\sigma \sim T^{-2}$ temperature dependence[3a] down to ca. 80 K, at which point a smooth metal-to-semiconductor transition occurs.[3d] Interestingly, the polycrystalline samples of $([Si(Pc)O]I_{1.12})_n$ also exhibit a significant but less pronounced decrease in $d\sigma/dt$ at higher temperatures (inset, Figure 23A). Such behavior is not evident for $([Ge(Pc)O]I_{1.08})_n$ samples. From these data and other comparisons of single-crystal vis-â-vis polycrystalline compaction conductivity data in low-dimensional materials,[3,4,12c,39] it is reasonable to anticipate that in the phthalocyanine stacking direction $([Si(Pc)O]I_{1.12})_n$ specimens will have a room-temperature conductivity on the order of ~100 Ω^{-1} cm^{-1} with modest "metal-like" temperature dependence. On the other hand, $([Ge(Pc)O]I_{1.08})_n$ samples will probably exhibit a stacking-axis room-temperature conductivity closer to ca. 10 Ω^{-1} cm^{-1} with a thermally activated temperature dependence.

Voltage-shorted compaction measurements offer a practical means to qualitatively sample transport characteristics in the high-conductivity direction of anisotropic materials by deliberately short-circuiting some of the effects of averaging over all crystallite

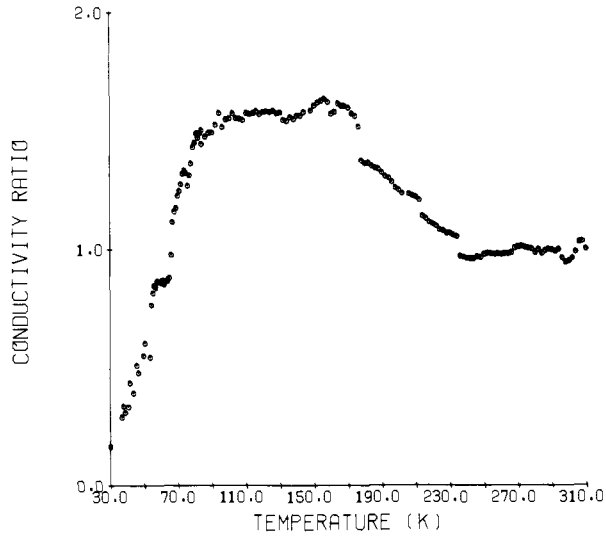

Figure 24. Voltage-shorted compaction conductivity data for a compacted powder sample of $([Si(Pc)O]I_{1.55})_n$ as a function of temperature.

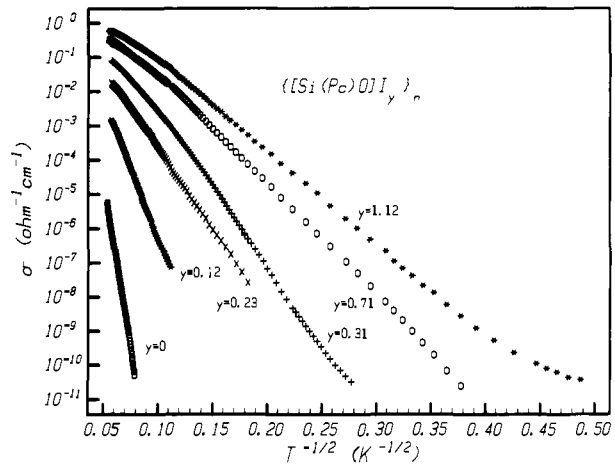

Figure 25. Variable-temperature electrical conductivity data for various polycrystalline $([Si(Pc)O]I_y)_n$ samples plotted in a log σ vs. $T^{-1/2}$ format.

orientations and interparticle contact resistance.[45] For the present materials, considerable difficulty was encountered in maintaining contact integrity at low temperatures (≲150 K). However, taken qualitatively, the results as exemplified by the $([Si(Pc)O]I_{1.55})_n$ data in Figure 24, indicate a "metal-like" transport behavior for Ni(Pc)I and $([Si(Pc)O]I_{1.12})_n$ in the region closer to room temperature but not for $([Ge(Pc)O]I_{1.08})_n$. Further studies to elucidate the behavior at lower temperatures are in progress.

The temperature dependence of $([M(Pc)O]I_y)_n$ conductivity was also studied as a function of y. As can be seen in Figures 21 and 22, for M = Si and Ge, incremental iodine doping not only increases the room-temperature conductivity but also results in a general diminution of the slopes of the log σ vs. $1/T$ lines. Similar behavior has been reported for other conductive organic polymers upon doping.[6,39,46] The functional form in which macromolecule conductivity depends upon temperature has been a subject of great discussion for doped polyacetylene, *p*-polyphenylene, and a number of other systems.[6,39,41a,46,47] In the present case, exhaustive attempts were made, via computer, to find the most appropriate mathematical fit to the experimental

(45) Coleman, L. B. *Rev. Sci. Instrum.* **1978**, *49*, 58–63.
(46) (a) Chance, R. R.; Shacklette, L. W.; Miller, G. G.; Ivory, D. M.; Sowa, J. M.; Elsenbaumer, R. L.; Baughman, R. H. *J. Chem. Soc., Chem. Commun.* **1980**, 348–349. (b) Audenaert, M.; Gusman, G.; Deltour, R. *Phys. Rev. B: Condens. Matter* **1981**, *B24*, 7380–7382 and references therein.
(47) Sichel, E. K.; Gittleman, J. I.; Sheng, P. *Phys. Rev. B: Condens. Matter* **1978**, *B18*, 5712–5716.

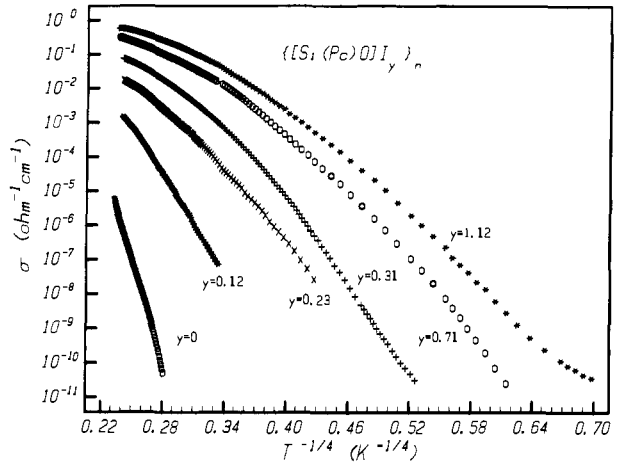

Figure 26. Variable-temperature electrical conductivity data for various polycrystalline $([Si(Pc)O]I_y)_n$ samples plotted in a log σ vs. $T^{-1/4}$ format.

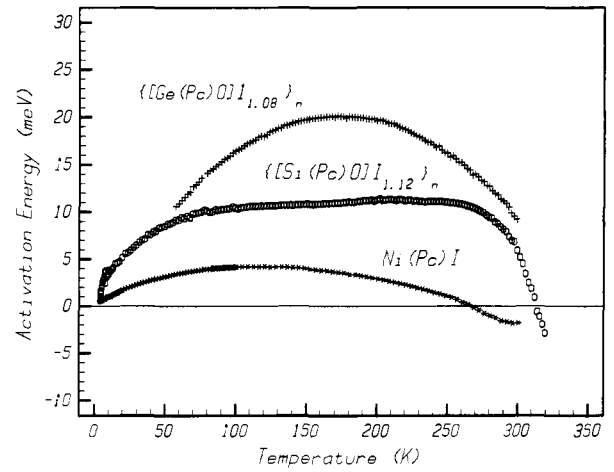

Figure 27. Activation energy vs. temperature for polycrystalline samples of $([Ge(Pc)O]I_{1.08})_n$, $([Si(Pc)O]I_{1.12})_n$, and Ni(Pc)I.

data. As exemplified in Figures 25 and 26, single exponential fits (eq 8) such as where $a = 0.50$ (associated with certain types

$$\sigma = Ae^{-(T_0/T)^a} \tag{8}$$

of tunneling between small metallic particles in an insulating medium, one-dimensional hopping, or certain types of disorder[10b,41c,47,48]) or $a = 0.25$ (variable-range hopping[42a,46b]) are not completely satisfactory over the entire temperature or doping range for $([Si(Pc)O]I_y)_n$ samples ($a = 0.6$ actually comes closest). Similar results were obtained for $([Ge(Pc)O]I_y)_n$.

A more satisfactory fit to the experimental data is obtained with a common[6] phenomenological model employing two different exponentials for high- and low-temperature regions (eq 9).

$$\sigma_{\text{high temp}} = Ae^{-(T_0/T)} \tag{9a}$$

$$\sigma_{\text{low temp}} = A'e^{-(T_0'/T)} \tag{9b}$$

Treating the T_0 parameters as phenomenological "activation energies," the parameters compiled in Table VII are derived from a least-squares fit to the experimental data. Of course, from the known transport behavior of Ni(Pc)I single crystals, and the transport similarities (activated conductivity at lower temperatures) in Ni(Pc)I, $([Si(Pc)O]I_y)_n$, and $([Ge(Pc)O]I_y)_n$ polycrystalline samples, it is obvious that the observed temperature dependence of the conductivity is probably not describable in terms of such a simple model and is strongly affected by the polycrystalline nature of the compacted powder samples. Indeed, that the two activation energy model is only an approximate description of the temperature dependence can be seen in Figure 27 where activation energy $(-kd(\ln \sigma))/d(1/T)$ is plotted against temperature for representative Ni, Si, and Ge samples. It can be seen that the activation energy tends to zero at 0 K, suggesting a limiting low-temperature conductivity in all three cases. Since the Ni(Pc)I powder conductivity remains as high as 5.5×10^{-3} Ω^{-1} cm^{-1} at 4.2 K, impurity conduction does not appear to be a dominant mechanism.

A charge-transport model which gives a more satisfactory fit to the variable-temperature data and which also necessarily involves a limiting low-temperature conductivity is based upon fluctuation-induced carrier tunneling through potential barriers separating metallic regions.[41a,47,48] In this case, the limiting low-temperature conductivity would occur via residual elastic tunneling.[48a] For a parabolic potential barrier, the conductivity can be expressed as in eq 10,[48a] where T_1 is an effective barrier

$$\sigma = \sigma_0 e^{-[T_1/(T+T_0)]} \tag{10}$$

activation energy. As can be seen in Figure 28, the fit of experimental $([Si(Pc)O]I_y)_n$ data to the model for a wide range of stoichiometries is rather good, with the only significant deviation being in samples where "metal-like" transport is observed at higher temperatures. The same situation obtains for Ni(Pc)I and $([Ge(Pc)O]I_{1.08})_n$ data (Figure 29). The low-temperature linear behavior of these plots is clearly in agreement with eq 10. The high-temperature "bendover" in the most conductive samples is

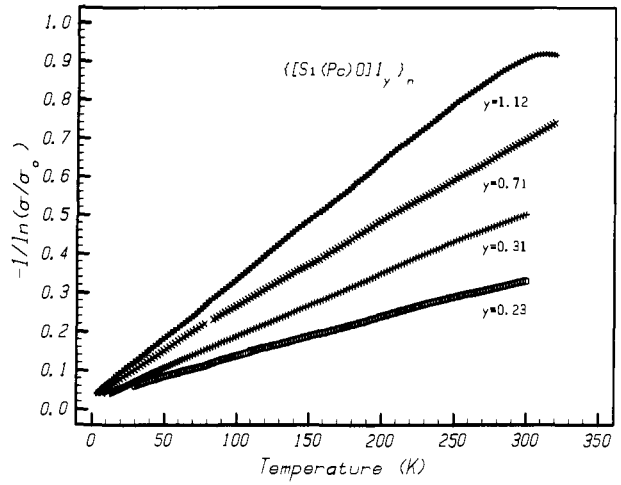

Figure 28. Conductivity data for the $([Si(Pc)O]I_y)_n$ system plotted as $-1/\ln(\sigma/\sigma_0)$ vs. T to illustrate correspondence with the fluctuation-induced tunneling model (eq 10).

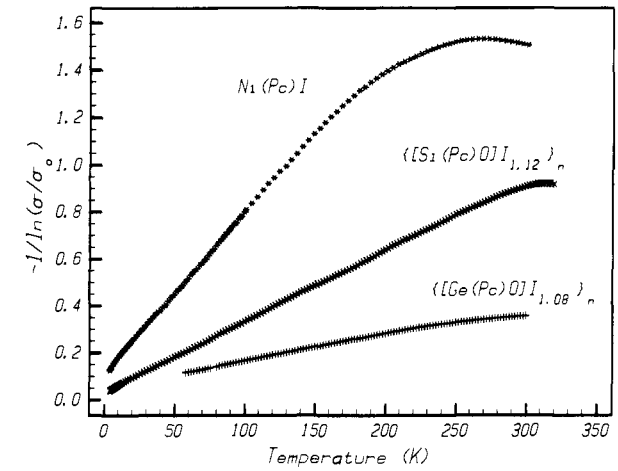

Figure 29. Conductivity data for polycrystalline Ni(Pc)I, $([Si(Pc)O]I_{1.12})_n$, and $([Ge(Pc)O]I_{1.08})_n$ samples plotted in accordance with the fluctuation-induced tunneling model (eq 10).

(48) (a) Sheng, P. *Phys. Rev. B: Condens. Matter* **1980**, *B21*, 2180–2195. (b) Mott, N. F. "Metal-Insulator Transitions"; Taylor and Francis: London, 1974; pp 30–42. (c) Movaghar, B.; Schirmacher, W. *J. Phys. C* **1981**, *14*, 859–880.

Table VIII. Fluctuation-Induced Tunneling Analysis Results[a]

compd	σ_0, Ω^{-1} cm^{-1}	T_1, °K	T_0, °K	$WA^{-1/5}$(Å$^{3/5}$)	$V_0A^{1/2}$, eV Å
$([Si(Pc)O]I_{0.23})_n$	0.35 (3)	973 (25)	32 (2)	16.1	5.5
$([Si(Pc)O]I_{0.31})_n$	0.56 (3)	619 (11)	14.8 (8)	22.7	5.2
$([Si(Pc)O]I_{0.71})_n$	1.24 (1)	428 (2)	14.4 (3)	18.6	3.9
$([Si(Pc)O]I_{1.12})_n$	1.74 (3)	330 (3)	9.5 (3)	22.2	3.8
$([Si(Pc)O]Br_{1.12})_n$	2.59 (1)	297 (1)	9.7 (1)	20.5	3.4
$([Ge(Pc)O]I_{1.08})_n$	1.8 (5)	827 (81)	38 (7)	12.7	4.5
Ni(Pc)I	15.3 (1)	146 (1)	15.8 (2)	9.1	1.6

[a] Calculated from a least-squares fit to eq 10 (see text).

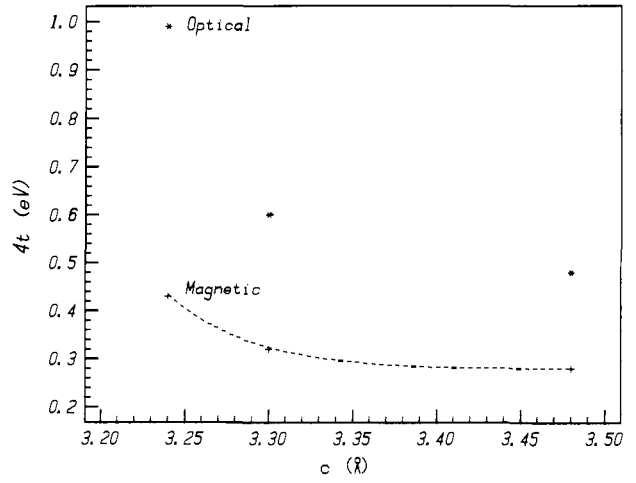

Figure 30. Derived Ni(Pc)I and $([M(Pc)O]I_y)_n$ bandwidths plotted vs. interplanar spacing.

as predicted[48a] for samples with intrinsic "metal-like" ($d\sigma/dt < 0$) behavior at sufficiently high temperatures. Parameters derived from a least-squares fit of the data (the linear portions) to eq 10 are compiled in Table VIII.

The parameters T_1 and T_0 can be expressed[38a] as in eq 11 and 12, where V_0 is the barrier height, A is the barrier cross-section

$$T_1 = \frac{2AV_0^2}{\pi e^2 kW} \tag{11}$$

$$T_0 = \frac{4\hbar AV_0^{3/2}}{\pi^2 e^2 kW^2 (2m)^{1/2}} \tag{12}$$

area (in Å^2), W is the barrier thickness (in Å), k is the Boltzmann constant, and m is the effective carrier mass. A priori, V_0 and W are calculable if A can be estimated[41a] by some independent means. In the present case, however, the systems appear sufficiently complex that we have chosen simply to express V_0 and W in units of A, as shown in Table VIII. Interestingly, it can be seen that the derived parameters all fall within a relatively restricted range, suggesting some constance in A. For the $([Si(Pc)O]X_y)_n$ system, the barrier parameters are especially close, suggesting in accord with the inhomogeneous doping and fit to a percolation model, that incremental halogenation (iodine *or* bromine) primarily increases the concentration of tunnel junctions and not their basic character.

Discussion

The investigation of the undoped and doped cofacially joined $[M(Pc)O]_n$ materials was undertaken with the dual goals of developing new control over the structures of low-dimensional electrically conductive molecular materials as well as investigating new, rational approaches to the synthesis of electrically conductive macromolecules. In the process, the present study and results to be reported in the future[3d,12a,49] shed new light on the properties of both types of materials.

In regard to low-dimensional systems composed of single molecules (and especially those composed of metallomacrocycles[3,13,14,23b,49-52]), the present work provides an informative picture of how collective properties respond to changes in interplanar, molecule–molecule spacings (3.24 → 3.30 → 3.48 Å) with all other molecular parameters held relatively constant. Furthermore, the unique opportunity to acquire complementary, small-molecule electronic structural information on dimers (A)

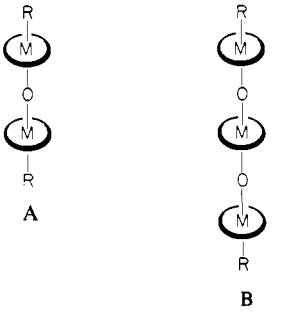

and trimers (B) which are, in reality, fragments of the polymer stack,[53,54] renders the cofacial assembly approach all the more attractive. Lastly, the present results present an interesting comparison to pressure-dependent studies of low-dimensional molecular systems in which collective properties are measured[55,56] at various interplanar spacings which are *less* than the normal, atmospheric pressure contacts.

Two aspects of molecular/macromolecular structure and oxidation state emerge in the present study and merit discussion. First, in the absence of halogen oxidation, the $[M(Pc)O]_n$ structure, M = Si and Ge, possesses eclipsed phthalocyanine rings at large interplanar spacings and staggered phthalocyanine rings at smaller interplanar spacings (in agreement with results on model compounds). However, upon partial oxidation, both systems are converted to an architecture with staggered rings, regardless of interplanar spacing. The driving force for this conformational change, which will be discussed in detail elsewhere,[53] can be largely ascribed to preferential, net *bonding* overlap between neighboring

(49) (a) Doris, K.; Ellis, D. E.; Marks, T. J.; Ratner, M. A., submitted for publication. (b) Inabe, T.; Jaggi, N. K.; Lyding, J. W.; Schneider, O.; Hanack, M.; Kannewurf, C. R.; Marks, T. J., Schwartz, L. H., submitted for publication.

(50) Dibenzotetraazaannulenes: (a) Lin, L.-S.; Marks, T. J.; Kannewurf, C. R.; Lyding, J. W.; McClure, M. S.; Ratajack, M. T.; Wang, T.-C. *J. Chem. Soc., Chem. Commun.* **1980**, 954–955. (b) Lin, L.-S.; Lyding, J. W.; Kannewurf, C. R.; Marks, T. J., submitted for publication.

(51) Porphyrins: (a) Martinsen, J.; Pace, L. J.; Phillips, T. E.; Hoffman, B. M.; Ibers, J. A. *J. Am. Chem. Soc.* **1982**, *104*, 83–91. (b) Phillips, T. E.; Scaringe, R. P.; Hoffman, B. M.; Ibers, J. A. *Ibid.* **1980**, *102*, 3435–3444.

(52) Hemiporphyrazines: (a) Dirk, C. W.; Mintz, E. A.; Schoch, K. F., Jr.; Marks, T. J. *J. Macromol. Sci., Chem.* **1981**, *A16*, 275–298. (b) Dirk, C. W.; Marks, T. J., manuscript in preparation. (c) Stojakovic, D. R.; Marks, T. J., unpublished results.

(53) (a) Doris, K.; Pietro, W. J.; Fragalà, I.; Marks, T. J.; Ratner, M. A., manuscript in preparation. (b) Doris, K.; Herbstein, F. H.; Marks, T. J.; Ratner, M. A., manuscript in preparation.

(54) Hush, N. S.; Cheung, A. S. *Chem. Phys. Lett.* **1977**, *47*, 1–4.

(55) (a) Jerome, D. in ref 4b; pp 123–142. (b) Debray, D.; Millet, R.; Jerome, D.; Barisic, S.; Giral, L.; Fabre, J. M. *J. Phys. Lett. (Orsay, Fr.)* **1977**, *38*, L227-L231.

(56) (a) Cooper, J. R. *Phys. Rev. B: Condens. Matter* **1979**, *B19*, 2404–2408 and references therein. (b) Welber, B.; Seiden, P. E.; Grant, P. M. *Ibid.* **1978**, *B18*, 2592–2700 and references therein. (c) Jérome, D.; Soda, G.; Cooper, J. R.; Fabre, J. M.; Giral, L. *Solid State Commun.* **1977**, *22*, 319–325.

metallomacrocycle π electron systems in the partially oxidized stack. Experimental support for the net bonding character of this interaction is also provided by the apparent contraction in the M(Pc)–M(Pc) interplanar spacings upon oxidation which was noted in the aforementioned diffraction results. Concerning the relationship between degree of partial oxidation and interplanar spacing, the $([M(Pc)O]I_y)_n$ materials stand in marked contrast to most other low-dimensional systems (e.g., TTF–TCNQ) where *decreasing* interplanar separations (e.g., pressure induced) result in *increased* charge transfer.[38e,57] As nearly as can be judged from the analytical data and resonance Raman spectra, increasing M(Pc) interplanar spacing provides additional accommodation for I_3^- counterions in the present systems, thus allowing *increased* partial oxidation (an alternative would be the formation of I_5^- counterions,[13,14] which would allow increased iodine uptake without increased oxidation). Of course, it is not possible to rule out metal ion effects, although the gas-phase ionization potentials of Ni(Pc)[3b] and various $M(Pc)X_2$ species,[53a] M = Si and Ge, are virtually identical.

The present study also reveals that essentially all $M(Pc)^{\rho+}$ carrier related collective properties are significantly sensitive to the ring–ring interplanar spacings. Thus, the static magnetic susceptibility, which is surprisingly temperature independent at all spacings (arguing that such behavior does not require "molecular metallic" conductivity), shows increasing "unpairing" of spins as the phthalocyanine plane–plane separation is increased (π orbital overlap decreased). To the extent that these data are amenable to analysis as Pauli-like via a tight-binding band description, "magnetic" bandwidths ($4t$) can be extracted. As can be seen in Figure 30, these vary in a nonlinear fashion with $\Delta c/c$ contraction (Ge → Ni). Analysis of optical reflectance data, with a pragmatic assumption of a simple free electron Drude model, also yields tight binding bandwidths. These "optical" bandwidths are in qualitative accord with the magnetically derived parameters (they are somewhat larger), and the functional dependence on interplanar spacing is roughly parallel (Figure 30). The magnitudes of the $([Si(Pc)O]I_{1.12})_n$ $4t$ obtained from magnetic and optical measurements, 0.32 and 0.60 eV, respectively, can be compared with a value of 0.62 eV, obtained from twice the measured splitting ($2t$ assuming negligible relaxation effects) of the HOMO ionization signal in the gas-phase He–I photoelectron spectra of analogous dimers (A, M = Si).[53,54] That the magnetically derived bandwidth parameters are perhaps too small may reflect Coulomb enhancement of the susceptibility (large U)[29b] or band perturbations arising from certain electron–phonon interactions.[58]

Although the electrical conductivities in the $([Si(Pc)O]I_y)_n$ and $([Ge(Pc)O]I_y)_n$ stacking directions could not be measured directly, established empirical correlations between single-crystal and pressed-powder data afford a reasonable estimation of these values and allow a qualitative comparison with the Ni(Pc)I data. These results evidence a greater sensitivity of the charge transport to interplanar spacing than found for the magnetic and optical bandwidths; again, the relationship is not a linear one (Figure 31A).

As already noted, the only other experiments to probe the properties of low-dimensional, stacked molecular conductors as a function of interplanar spacing have been those employing high pressures (up to 60 kbar).[55,56] Although such experiments involve multiaxial changes in lattice parameters and involve contractions below the natural (1 bar) spacings, they still complement the present data in an informative way. In Figure 31B are plotted the present normalized bandwidths vs. interplanar contraction (Ge → Ni) and normalized optical bandwidths for TTF–TCNQ (the curve for TSeF–TCNQ is nearly super imposable) obtained from pressure-dependent studies,[59a] plotted vs. stacking axis contraction.[56b,59b] Unfortunately, the TTF–TCNQ magnetic data[56c] do not extent over a sufficiently large pressure range to obtain a comparable $\Delta c/c$ variation. Since the TTF–TCNQ and TSeF–TCNQ bandwidth data involve contributions from both donor and acceptor stacks, Figure 31B also incorporates calculated[38f,60] $X\alpha$ scattered wave bandwidths for TTF and TCNQ stacks as a function of interplanar separation. It can be seen that the interplanar spacing dependence of the derived $M(Pc)^{\rho+}$ bandwidth is steeper than for either of the two organic materials (under pressure). This relationship probably reflects the fact the plane–plane distances in the germanium, and perhaps to a lesser extent silicon, polymers are likely at the limit of significant π orbital overlap.[61] However, the less diffuse character of the phthalocyanine carbon and nitrogen π orbitals vs. those of sulfur and selenium[60] may also impart greater "steepness". This is evident in the greater calculated sensitivity of TCNQ bandwidths to interplanar spacing than those of TTF or TSeF.[60]

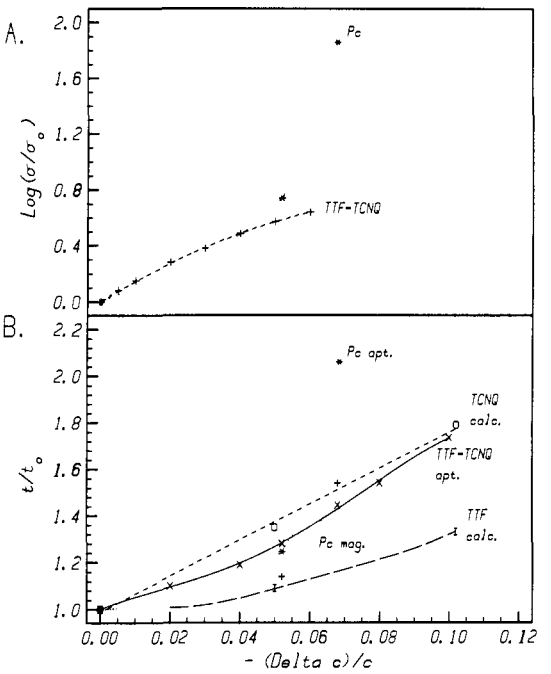

Figure 31. (A) Normalized electrical conductivities for phthalocyanine materials and TTF–TCNQ (b axis) as a function of the contraction in lattice spacing. (B) Normalized transfer integrals as a function of lattice spacing contraction: (*) phthalocyanine materials (optical data); (+) phthalocyanine materials (magnetic data); (×) TTF–TCNQ (optical data of ref 56b), (○) TTF–TCNQ, TCNQ stack ($X\alpha$ calculations of ref 60); (I) TTF–TCNQ, TTF stack ($X\alpha$ calculations of ref 60).

In regard to understanding the properties of acceptor-donor conductive organic polymers, the $([M(Pc)O]I_y)_n$ and $([M(Pc)O]Br_y)_n$ materials also provide an informative perspective. A number of physical changes which commonly occur upon doping delocalized organic polymers are manifestations in the present case simply of an inhomogeneous doping process involving two phases (one conductive, one essentially insulating) of well-defined structure and stoichiometry. Thus, increasing Pauli-like paramagnetism upon incremental doping, increasing reflectivity upon incremental doping, the relationship of σ and y, falling activation energy for conductivity with increasing y, and the unusual relationship of σ to temperature are all observed and can be understood

(57) (a) Conwell, E. M. *Solid State Commun.* **1980**, *33*, 17–19. (b) Torrance, J. B.; Vazquez, J. E.; Mayerle, J. J.; Lee, V. Y. *Phys. Rev. Lett.* **1981**, *46*, 253–257.

(58) Marianer, S.; Weger, M.; Gutfreund, H., submitted for publication. We thank Professor Weger for a preprint and a stimulating discussion.

(59) (a) Bandwidths were calculated assuming $4t \propto \omega_p^2$. (b) Since the stacks in TTF–TCNQ are slipped, the contraction plotted ($\Delta c/c$) is the change in molecule repeat distance along the monoclinic b axis.

(60) Herman, F. *Phys. Scr.* **1977**, *16*, 303–306.

(61) Interestingly, the magnitude of an analogous, photoelectron spectroscopy derived "through space" interaction parameter in cyclophanes appears to be almost linearly dependent on interplanar spacing from ca. 3.38 Å (0.5 eV) to ca. 2.65 Å (1.4 eV): (a) Kovac, B.; Mohraz, M.; Heilbronner, E.; Boekelheide, V.; Hopf, H. *J. Am. Chem. Soc.* **1980**, *102*, 4314–4324. (b) Kovac, B.; Allan, M.; Heilbronner, E. *Helv. Chim. Acta* **1981**, *64*, 430–448.

in terms of largely inhomogeneous doping, without invoking more elaborate doping–electronic structure relationships.

It is evident that the cofacial assembly strategy offers new means, via stringent structural control, to probe the nature of those factors which stabilize the molecular metallic state. Building upon the methodology and results outlined in the present study, experiments directed at elucidating dopant electronic vs. structural effects, the influence of stack length, the effect of macrocycle and macrocycle substituents, as well as further manipulation of interplanar spatial relationships are logical extensions of the work. In regard to extended molecular arrays, it should also be evident that this strategy offers the possibility of assembling an almost limitless variety of electrically conductive macromolecules. Further efforts at characterizing and processing the most interesting of these materials are in progress.[62]

Acknowledgment. This research was generously supported by the Office of Naval research (to T.J.M.) and by the NSF-MRL program through the Materials Research Center of Northwestern University (Grant DMR79-23573). We thank Professor M. T. Ratajack for helpful discussions concerning the analysis of reflectivity data, Professor J. B. Cohen and Dr. P. Georgopoulos for access to the X-ray diffraction equipment as well as helpful advice, and D. Keszler for helpful advice on the use of LAZY PULVERIX.

Registry No. Ni(Pc)I, 84624-83-9; $[Si(Pc)O]_n$, 39114-20-0; $[Ge(Pc)O]_n$, 55948-70-4; $[Sn(Pc)O]_n$, 57156-42-0.

(62) (a) Inabe, T.; Lyding, J. W.; Moguel, M. K.; Marks, T. J. *J. Phys.*, in press. (b) Dirk, C. W.; Inabe, T.; Lyding, J. W.; Schoch, K. F., Jr.; Kannewurf, C. R.; Marks, T. J. *J. Polymn. Sci., Polym. Chem. Ed.*, in press.

Kinetic Features of an Intraresin Reaction[1]

Bong Kim, Piotr Kirszensztejn, Durgadas Bolikal, and Steven L. Regen*

Contribution from the Department of Chemistry, Marquette University, Milwaukee, Wisconsin 53233. *Received August 10, 1982*

Abstract: The kinetic features of the intraresin displacement by pendant ammonium acetate groups on chloromethylated polystyrene have been investigated as a function of temperature, swelling solvent, and cross-link density. In all cases, intraresin displacement proceeds with a rapid initial rate followed by a very slow second stage; the latter represents that fraction of reactants which become "kinetically isolated". The free energy of activation for the first stage, under the various swelling conditions used, lies in the range 24.4–26.8 kcal mol^{-1}, which is similar to that found for analogous homogeneous reactions. The absolute rates measured for the homogeneous and the initial intraresin displacement in dioxane were similar; with *n*-hexane and toluene as solvents, polymeric rates were considerably slower than those of their homogeneous counterparts. Intraresin displacement was rapid even when a poor swelling solvent (*n*-hexane) was used. As the rate of intrapolymeric reaction decreased (through a decrease in temperature, increase in cross-link density, or change in solvent), the percent of "kinetically isolated" sites increased.

The study of "site–site interactions" in cross-linked polymers has attracted considerable interest over the past 12 years.[2,3] Surprisingly, however, very little attention has focused on the rates of such processes.[4] In this paper we report the first direct kinetic study of an intraresin reaction, i.e., the intrapolymeric displacement by pendant ammonium acetate on chloromethylated polystyrene (eq 1). Our reasons for choosing this specific system for investigation were 3-fold. First, a simple nucleophilic displacement such as this should have a significant activation energy. While "kinetic isolation" within cross-linked polymers has been clearly demonstrated for the dimerization of *o*-benzyne[4] its existence has not been rigorously proven for reactions which possess appreciable energy barriers. Second, reaction 1 proceeds without a change in cross-link density and charge concentration. Since each of these factors can influence "site-isolation" effectiveness, both should be constant in any resin system designed for kinetic study.[5,6]

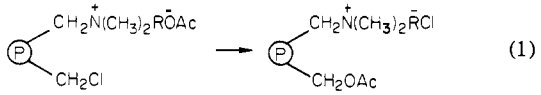

(1)

Table I. Influence of Onium Salt Structure, Temperature, and Solvent on the Rate of Homogeneous Displacement

$PhCH_2N(CH_3)_2R^+ OAc^- + PhCH_2Cl \rightarrow PhCH_2N(CH_3)_2R^+Cl^- + PhCH_2OAc$

R	solvent	temp, °C	10^5-k_2, M^{-1} s^{-1}	$\Delta H^{\ddagger}$, kcal mol^{-1}	$\Delta S^{\ddagger}$, eu	$\Delta G^{\ddagger}$ at 333.15 K, kcal mol^{-1}
n-C_4H_9	dioxane	60	499	14.1	−27.3	23.1
		50	277			
		40	121			
n-$C_{16}H_{33}$	dioxane	60	522	16.5	−19.8	23.1
		50	400			
		40	100			
n-$C_{16}H_{33}$	toluene	60	200	18.7	−15.0	23.7
		50	100			
		40	32			
n-$C_{16}H_{33}$	*n*-hexane	60	350	12.0	−33.9	23.3
		50	170			
		40	100			

(1) Supported by the Division of Basic Energy Sciences of the Department of Energy (Contract EG 77-S-02-4446) and the donors of the Petroleum Research Fund, administered by the American Chemical Society.

(2) A preliminary account of this work has been published: Regen, S. L.; Bolikal, D. *J. Am. Chem. Soc.* **1981**, *103*, 5248.

(3) For recent reviews of "site–site interactions", see: Kraus, M. A.; Patchornik, A. *Macromol. Rev.* **1980**, *15*, 55. Kraus, M. A.; Patchornik, A. *Isr. J. Chem.* **1978**, *17*, 298. Crowley, J. I.; Rapoport, H. *Acc. Chem. Res.* **1976**, *135*. Hodge, P.; Sherrington, D. C. "Polymer-Supported Reactions in Organic Synthesis"; Wiley: New York, 1980. Mathur, N. K., Narang, C. K.; Williams, R. E. "Polymers as Aids in Organic Chemistry"; Academic Press: New York, 1980.

(4) Mazur, S.; Jayalekshmy, P. *J. Am. Chem. Soc.* **1979**, *101*, 677. Rebek, J., Jr.; Trend, J. E. *Ibid.* **1979**, *101*, 737.

(5) Chang, Y. H.; Ford, W. T. *J. Org. Chem.* **1981**, *46*, 5364.

(6) Regen, S. L.; Lee, D. P. *J. Am. Chem. Soc.* **1974**, *96*, 294.

0002-7863/83/1505-1567$01.50/0